# The Tibetan Plateau Space-based Tropospheric Aerosol Climatology: 2007–2020

Honglin Pan[1,2], Jianping Huang[1]*, Jiming Li[1], Zhongwei Huang[1], Minzhong Wang[2], Ali Mamtimin[2], Wen Huo[2], Fan Yang[2], Tian Zhou[1], Kanike Raghavendra Kumar[3]

[1]*Collaborative Innovation Center for Western Ecological Safety, College of Atmospheric Sciences, Lanzhou University, Lanzhou, 730000, China*

[2]*Institute of Desert Meteorology, China Meteorological Administration, National Observation and Research Station of Desert Meteorology, Taklimakan Desert of Xinjiang, Taklimakan Desert Meteorology Field Experiment Station of China Meteorological Administration, Xinjiang Key Laboratory of Desert Meteorology and Sandstorm, Key Laboratory of Tree-ring Physical and Chemical Research, China Meteorological Administration, Urumqi, 830002, Xinjiang, China*

[3] *Department of Engineering Physics, College of Engineering, Koneru Lakshmaiah Education Foundation, Vaddeswaram, Guntur 522302, Andhra Pradesh, India*

Correspondence: Jianping Huang (hjp@lzu.edu.cn)

**Abstract.** A comprehensive and robust dataset of tropospheric aerosol properties is important for understanding the effects of aerosol-radiation feedback on the climate system and reducing the uncertainties of climate models. The third pole of Earth (Tibetan Plateau, TP) is highly challenging to obtain long-term in situ aerosol data due to its harsh environmental conditions. Here, we provide the more reliable new vertical aerosol index (AI) parameter from the spaceborne-based Lidar (CALIOP) of CALIPSO over TP during 2007-2020 for daytime and nighttime to investigate the aerosol's climatology. The calculated vertical AI was derived from the aerosol extinction coefficient (EC), which was rigorously quality-checked and validation, strictly quality checked, and validated for passive satellite sensors (MODIS) and ground-based LIDAR measurements. Generally, our results demonstrate the agreement of the AI dataset with the CALIOP and ground-based LIDAR. Besides, the results show that after removing the low-reliability aerosol target signal, the optimized data can obtain the aerosol characteristics with higher reliability. Our data set also reveals the patterns and concentrations of high-altitude vertical structure characteristics of the tropospheric aerosol over the TP. Our dataset will help to update and makeup the observational aerosol data in the TP. We encourage climate modeling groups to consider new analyses of the AI vertical patterns, comparing the more accurate datasets, with the potential to increase our understanding of the aerosol-cloud interaction(ACI) and aerosol-radiation interaction (ARI) and its climate effects. Data described in this work are available at https://data.tpdc.ac.cn/en/disallow/03fa38bc-25bd-46c5-b8ce-11b457f7d7fd
DOI:10.11888/Atmos.tpdc.300614. (Honglin Pan et al., 2023).

**Keywords:** Tibetan Plateau, Aerosol index vertical structure, Tropospheric aerosols, Aerosol climatology

## 1 Introduction

The three poles (i.e., the Arctic, Antarctic and Tibetan Plateau (TP)) have the highest mountains in the world and store more snow, ice and fresh water than any other place. The unique geographical location of the Antarctic, Arctic, and TP, as the unique ecological, climatic, and natural environmental changes, have crucial role in global and regional climate change. However, studies have found that these regions are susceptible to climate change and that their differences may also affect key feedback loops for global climate change and the sustainability of human societies. Unfortunately, our understanding of the three poles, particularly the relations between the regions, remains limited due to insufficient observation data. Currently, the collection of additional research data for these extreme environments is one of the major bottlenecks in facilitating comprehensive studies of these regions. Sufficient attention has been given to the polar regions and the TP in successive IPCC reports (IPCC, 2013 and 2021). The similarities between TP and the other two polar regions are their low temperatures, remote location, and large water storage capacity. On the other hand, TP has a more highly complex climate than the Arctic and Antarctic (where ice is the primary medium) and its land surface (including forests, grasslands, bare soil, lakes and glaciers) is more diverse. These differences make the transport and accumulation of pollutants in the TP region different from the other two polar regions.

TP, is known as the "Third Pole" because it has the third largest ice mass on Earth, after the Antarctic and Arctic regions (Qiu, 2008). TP is also called the "Asia Water Towers", provides fresh water to 40% of the world's population due to its vast water reserves such as glaciers, lakes and rivers (Immerzeel et al., 2010). Furthermore, TP is the "Roof of the World", which covers an area of ~2.5 million $km^2$ at an average altitude of about 4,000 m a.s.l. (above sea level) and includes all of Tibet and parts of Qinghai, Gansu, Yunnan, and Sichuan in southwestern China, as well as parts of India, Nepal, Bhutan, and Pakistan (Nieberding et al., 2020). To the north of the TP region is situated by Taklamakan Desert (TD) (see Figure 1). This high altitude and specific topographic area effectively serve as a heat source during the spring and summer months. This

90    thermal structure helps the TP to function virtually as an "air pump", attracting warm

91    and humid air from the lower latitude oceans by suction (Yanai et al., 1992; Wu and

92    Zhang, 1998; Wu et al., 2007; Wu et al., 2012). Consequently, large-scale mountains

93    play a crucial role in shaping regional and even global weather and climate through

94    mechanical and thermodynamic effects and affect the global energy-water cycle (Xu et

95    al., 2008; Molnar et al., 2010; Boos and Kuang, 2010; Wu et al., 2015). It is closely

96    related to the survival of human beings in the world.

97      Climate projections are simulated responses of the climate system to future

98    emission or concentration scenarios of greenhouse gases (GHGs) and aerosols and are

99    generally calculated using climate models. The reasons for the gap between models and

100   observations may also be due to inadequate solar, volcanic, and aerosol forcing used in

101   the models, and in some modeling, may be due to an overestimation of the response to

102   increasing GHG and other anthropogenic forcing (the latter reason includes mainly the

103   role of aerosols). The most significant uncertainties in predicting future climate change

104   are related to uncertainties in the distribution and properties of aerosols and clouds,

105   their interactions, and limitations in the representation of aerosols and clouds in global

106   climate models (IPCC, 2021). The primary aerosol type over the TP is dust, which is

107   primarily contributed to the Taklimakan Desert (Liu et al.,2008; Chen et al., 2013;2022;

108   Xu et al., 2015). Previously some studies of aerosol-cloud interaction(ACI) and aerosol-

109   radiation interaction(ARI) have been conducted. For example, the dust aerosols lifting

110   over the TP reduce the radius of ice particles in the convective clouds over the TP and

111   prolong the cloud lifetime through the indirect radiation effect, which can lead to the

112   development of higher convective clouds. The dust-affected convective clouds move

113   further eastward under the action of westerly winds and merge with local convective

114   cloud masses, triggering heavy precipitation in the Yangtze River basin and northern

115   China downstream of the TP (Liu et al., JGR, 2019; Liu et al., NSR,2019). However,

116   the effect of aerosol on the atmospheric energy and water cycle remains uncertain,

117   mainly due to lacking long-term and accurate vertical aerosol optical properties dataset

118   over the TP. This can help better understand aerosol's impact on the atmospheric heating

119   rate and stabilization and the subsequent cloud-precipitation process. Therefore,

120  constructing a more long-term and reliable vertically dataset of aerosol optical

121  parameters can make up the observational facts for aerosol-related study and provide a

122  scientific basis for improving the global climate model simulation over the TP.

123     Generally, the primary aerosol optical characteristic parameters (such as extinction

124  coefficient (EC), aerosol optical depth (AOD)) acquisition method is in situ

125  observations, which have high precision. However, in situ observations are restricted

126  by the distribution of observation stations over TP. Hence, the resulting data lack spatial

127  continuity, making it difficult to use to meet the objectives of growing regional

128  atmospheric environmental studies (Chen et al.,2022; Goldberg et al.,2019; Giles et al.,

129  2019). Satellite remote sensing (active and passive) is an effective tool for collecting

130  aerosol optical information (including the vertical structure and spatial distribution)

131  over a wide range of spatial scales, significantly offsetting the deficiencies of in situ

132  observations. Satellite remote sensing can tackle difficulties connected to insufficient

133  data and uneven geographical distributions to a certain extent (Chen et al., 2022; Wei

134  et al.,2021). While for aerosol products from CALIPSO, the presence of some low-

135  reliability aerosol target (LRAT) caused by cloud contamination, solar noise

136  contamination, especially in the daytime, and ground clutter among mostly aerosol

137  observations skews the distribution of the aerosol EC toward larger values, at least some

138  of which may be identified as aerosols and retained in the analysis, makes the presence

139  of some low confidence aerosol targets bias the distribution of aerosol extinction in

140  most aerosol observations. The distribution of the aerosol EC will show greater biased

141  values (Thomason and Vernier, 2013; Kovilakam et al., 2020; Pan et al., 2020; Kahn et

142  al., 2010), and then will further enhance the aerosol index (AI) value due to the

143  influence of radiation transfer interaction between clouds and the absorption layer,

144  which will not truly reflect the differences in aerosol physical properties (Guan et al.,

145  2008; Liu et al., 2019; Kim et al.,2018). Hence, gaining high confidence in EC helps us

146  analyze aerosol optical properties and better lead to numerous pertinent uses of EC data,

147  is essential for accurately characterizing the upper range of aerosol ECs that occur on

148  the TP.

149     The present study provides a dataset of monthly average vertical structure

150 characteristics of tropospheric high confidence aerosol optical properties including EC,

151 AOD, Angstrom exponent (AE), aerosol index (AI) between the daytime and nighttime

152 over the TP and surrounding areas. The data for the above-mentioned optical properties

153 were retrieved based on the space-borne Lidar CALIOP data (Cloud-Aerosol Lidar with

154 Orthogonal Polarization) from Cloud-Aerosol Lidar and Infrared Pathfinder Satellite

155 Observation (CALIPSO) satellite for the period 2007-2020. The main objective of this

156 study is to calculate new and high-confidence aerosol optical parameter of AI in the

157 vertical distribution, by the strict quality control and validation for passive satellite

158 sensor (MODIS) and ground-based LIDAR. Since AI is dependent on aerosol

159 concentration, optical properties and altitude of the aerosol layer, and AI is particularly

160 sensitive to high-altitude aerosols, which is used to indicate small particles (those that

161 act as cloud condensation nuclei) with a high weight (Guan et al., 2010; Buchard et al.,

162 2015; Liu et al., 2019; Nakajima et al., 2001). The comprehensive data set of aerosol

163 properties utilized in the study is of substantial importance for understanding the impact

164 of aerosol on the ecosystem and reducing the uncertainties of climate models.

165 The data set in this study can more effectively characterize the vertical structure

166 of aerosols while following standardized quality control methods to obtain higher

167 confidence in the aerosol vertical structural properties covariate data sets, and allow for

168 comparison and application to the study of climate models and other atmospheric

169 science related problems between our records and other public different data sets. To

170 ensure meaningful confidence estimates for the constructed aerosol covariates over the

171 TP, it is necessary to apply carefully the following correction procedures and analytical

172 validation. The main steps to construct the dataset are grouped as follows: (1) Removing

173 the low-confidence aerosol extinction coefficient for 532nm and 1064nm caused by the

174 misclassification of cloud and other interferences (e.g., surface clutter, hygroscopicity

175 etc.). Based on this, an interquartile range (IQR) method (see section 2.2) is utilized to

176 discard the low confidence targets, and further obtain the monthly average aerosol EC

177 for day and night with higher confidence; (2) the pseudo- Ångström exponent (hereafter

178 AE) is calculated using the EC at 532 and 1064nm with higher confidence; (3) obtaining

179 vertical AI by the product of the AOD (the vertical layers integral of EC) and AE. (4)

180    Validation for the constructed AI with: MODIS and in situ LIDAR measurements using

181    standardized frequency distributions.

182    **2 The construction of the data set**

183    **2.1 Study area**

184         Figure 1 depicts the geopotential height of the TP and its surrounding areas (27-

185    42°N,75-102°E, about 4,000 m a.s.l.), and schematic diagram of CALIPSO satellite

186    ground track over the TP in other months. The role of the "heat-driving air pump" of

187    the TP provides abundant water vapor for the formation of clouds (Luo et al., 1984;

188    Liou et al.,1986). Furthermore, the TP environment is greatly affected by natural and

189    anthropogenic aerosols from the surrounding regions (Chen et al., 2013; Bucci et

190    al.,2014; Xu et al.,2015). The strong convection generated by the TP will promote

191    aerosols' vertical transport and increase aerosols' content in the troposphere and

192    stratosphere (Vernier et al., 2015; Liu et al., 2022). Aerosols also serve as cloud

193    condensation nuclei (CCN) or ice nuclei (IN), modifying cloud structure properties and

194    precipitation (Twomey et al.,1977). Hence, the TP has been called the pumping pump

195    of water vapor, the clouds incubator, and the sand dust transfer station. By delivering

196    water vapor, clouds, and dust, it regulates extreme weather and climate in the

197    downstream and surrounding areas. It can be seen that the TP plays a crucial role in the

198    impact and regulation of global and regional climate or environments (Luo et al.,1984;

199    Rossow et al., 1999; Wan et al.,2017; Liu et al., 2022).

200

201

202

203

204

205

206

207

208

209

210

211

212
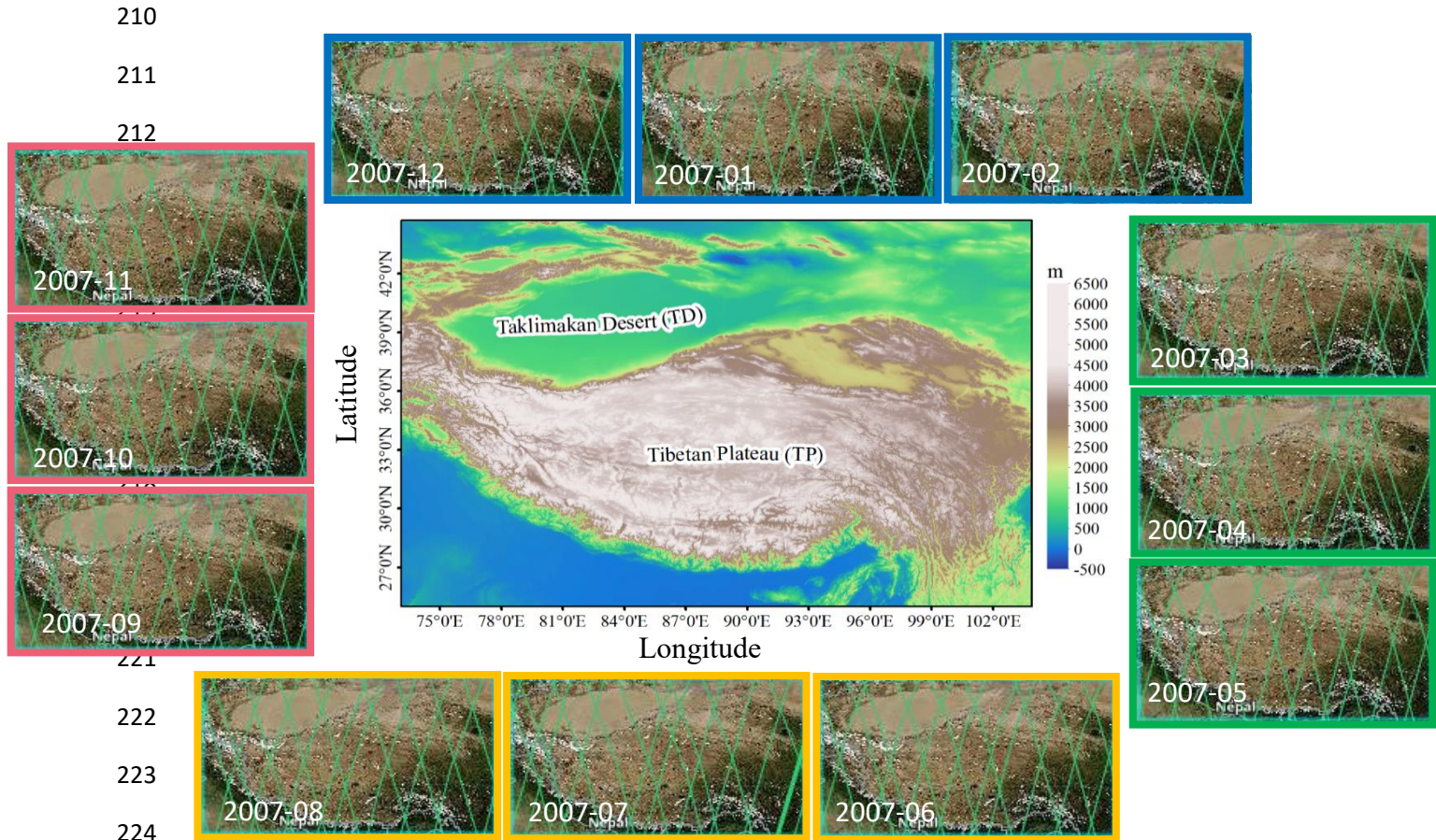
Figure. 1 The geopotential height of the TP and its surrounding areas (27-42°N,75-102°E), schematic diagram of the transit of CALIPSO satellite orbits over the TP in other months (with 2007 as an example. March-May is spring, June-August is summer, September-November is autumn, and December-February is winter).

**2.2 CALIPSO-CALIOP data and low-reliability aerosol target (LRAT) clearing method**

CALIPSO (Cloud-Aerosol Lidar and Infrared Pathfinder Satellite Observations) satellite was launched by NASA on 28 April 2006. The CALIOP (Cloud-Aerosol Lidar with Orthogonal Polarization) onboard CALIPSO is the nadir-pointing dual-wavelength polarization Lidar, which can provide the global and continuous information on the vertical distribution of aerosols and clouds at 532 nm and 1064 nm for daytime and nighttime (Winker e t al., 2007 and 2009). The CALIPSO-CALIOP (version 4.20) level-2 aerosol profile product is selected in this study, with vertical and horizontal resolutions of 60 m and 5 km, respectively. The used parameter includes Extinction_Coefficient_532 and Extinction_Coefficient_1064 between daytime and

nighttime from 2007 to 2020. It should be noted that CALIOP observation data uses as few instruments as necessary to complete the monthly aerosol climatology. We make this decision to limit the impact of differences between instruments due to measurement techniques and wavelength range as well as assess the general quality of the instrument's data set.

The presence of some low-reliability aerosol target (LRAT) caused by cloud contamination, solar noise contamination, especially in the daytime, and ground clutter among mostly aerosol observations skews the distribution of the aerosol EC toward larger values (Thomason and Vernier, 2013). Consequently, to eliminate the LRAT, a statistical approach to identify LRAT, and extreme outliers is utilized based on the interquartile range (IQR). IQR is a more conservative measure of the spread of distribution than standard deviation (Iglewicz and Hoaglin, 1993). Note that this technique is based on median statistics rather than the mean due to the skew distribution of EC. In our implementation, we use daily data at each altitude (0.06 km) and latitude (0.05°) bin from 2007-2020 to determine an EC frequency distribution for different months. Besides, we used the lower quartile (Q1) and upper quartile (Q3) of the underlying distribution to find IQR, defined as Q3-Q1, a good measure of the spread in the data relative to the median. Here, an extreme outlier is defined as Q3 + (3.5×IQR), and a more upper outlier (Q3+(1.5×IQR)) is used for comparison (Iglewicz and Hoaglin, 1993). Meanwhile, the extreme outlier threshold is used to clear LRAT-affected observations from the data set, which is better and more effective at identifying outliers in the density distribution (Kovilakam et al., 2020).

**2.3 AI Data processing**

According to the method described in section 2.2, the aerosol EC (observed at 532 nm and 1064 nm for daytime and nighttime) with higher reliability over the TP is obtained. The monthly mean Ångström exponent (hereafter "pseudo-Ångström exponent (AE)") between daytime and nighttime is derived to establish the 14-year aerosol climatology (2007-2020) based on equation (1). The AE model for EC wavelength dependence for 532 and 1064 nm is given by (Kovilakam et al., 2020):

$$EC_{-532[m,i,j]} = EC_{-1064[m,i,j]}\left(\frac{\lambda_{532}}{\lambda_{1064}}\right)^{AE[m,i,j]}$$

269                                                                              (1)

270  where EC_532 [m, i, j] and EC_1064 [m, i, j] are extinction coefficient at 532, and 1064 nm,

271  respectively; AE [m, i, j] is the pseudo-Ångström exponent (Rieger et al.,2015;2019);

272  and the indices [m, i, j] represent the month, latitude, and altitude respectively.

273  ($\lambda_{532}/\lambda_{1064}$) represents the ratio of wavelengths at 532 and 1064 nm. The AE is gridded

274  to 0.05° latitude and 0.06 km altitude resolution. Further, the vertical distribution of

275  the new parameter AI is calculated according to equation (2). AI has been developed by

276  (Nakajima et al., 2001; Liu et al., 2019):

277  $AI_{[m,i,j]} = AOD_{[m,i,j]} \times AE_{[m,i,j]}$                                                       (2)

278  where $AI_{[m,i,j]}$ and $AOD_{[m,i,j]}$ are aerosol index and aerosol optical depth, respectively;

279  $AE_{[m, i, j]}$ is the pseudo-Ångström exponent; and [m, i, j] represent the month, latitude,

280  and altitude respectively. Note that to match the AE, AOD is also transformed into the

281  vertical distribution (not the column parameter). As we focus on the characteristics of

282  aerosols in the troposphere over the TP, we took samples from the surface at an altitude

283  of 12km with a vertical resolution of 0.06km. We integrated the EC of each two layers

284  to obtain an AOD, which corresponds to the average of the AE values of each two layers.

285  This achieves spatial matching between AOD and AE at the vertical heights. In the later

286  stage, when using the AI obtained from MODIS for comparative testing, we used the

287  PDF and average values of AI for characterization display in order to facilitate

288  comparison due to the differences in horizontal and vertical space. The data in this

289  manuscript are all based on the vertical structural distribution of altitude-latitude with

290  vertical and horizontal resolutions of 60 m and 0.05°, respectively. The monthly mean

291  climatology of AI is computed in altitude and latitude for 532 and 1064nm between

292  daytime and nighttime.

293  **2.4 Aqua-MODIS data**

294      Like CALIPSO, Aqua is part of the A-Train constellation of satellites. Therefore,

295  MODIS (Moderate-resolution Imaging Spectroradiometer) onboard Aqua can achieve

296  near-simultaneous observations of clouds and aerosols with CALIPSO-CALIOP (less

than two minutes) (Winker et al., 2007; Hu et al., 2010). The Aqua satellite was successfully launched on May 4th, 2002. Aqua is the afternoon star, passing through the equator from south to north at around 13:30 local time. The observation data of 36 wavebands were obtained, with a maximum spatial resolution of 250 m and a scanning width of 2330 km. MODIS is a passive imaging spectroradiometer, there are a total of 490 detectors distributed in 36 spectral bands, with full spectral coverage ranging from 0.4 microns (visible light) to 14.4 microns (thermal infrared). In this study, Level 3 data (MYD08_M3) on a 1°×1° (longitude × latitude) gridded box is utilized. As shown in Table 1, MODIS can provide 550 nm AOD and AE products. It is worth mentioning that we chose this data because MODIS data is widely used and has certain reliability in aerosol research. The parameters of AE and AOD from MODIS are also used to calculate the AI, which is applied to evaluate the monthly mean climatology of AI from CALIOP over TP (see Table 1).

Table.1 Comparison between MODIS and CALIOP existing data products (√ represents the existing data products of the satellite, × represents data parameters that need further calculation in this study).

| Detector/Satellite | Wavelength | Extinction Coefficient (EC) | Aerosol Optical Depth (AOD) | Angstrom Exponent (AE) | Aerosol Index (AI) |
|---|---|---|---|---|---|
| CALIOP/CALIPSO (active) | 532&1064nm | √ | √ | × | × |
| MODIS/Aqua (passive) | 550nm | × | √ | √ | × |
| | | | | verification | verification |

## 2.5 Ground-based LIDAR data

Besides, we use the ground-based LIDAR (Light Detection and Ranging) (38.967 ° N, 83.65 ° E, 1099.3m) detection data from the hinterland of the Taklimakan Desert (TD) to verify the validity and accuracy of the low confidence aerosol removal method and the AI calculated by CALIOP detection data. Multi-band Raman polarization LIDAR (hereafter LIDAR) is mainly used for the detection of dust, aerosols, and clouds particles in the atmosphere, which detection belongs to "Belt and Road" Lidar Network

from Lanzhou University, China (http://ciwes.lzu.edu.cn/), has an advantage with calibrate or validate Satellite observation (see Figure 2). The primary technical specifications of LIDAR are as given in Table 2. For the performance of this LIDAR and the data inversion of aerosol related optical parameters, the authors advise the readers to refer the research work of Zhang et al. (2022 and 2023).
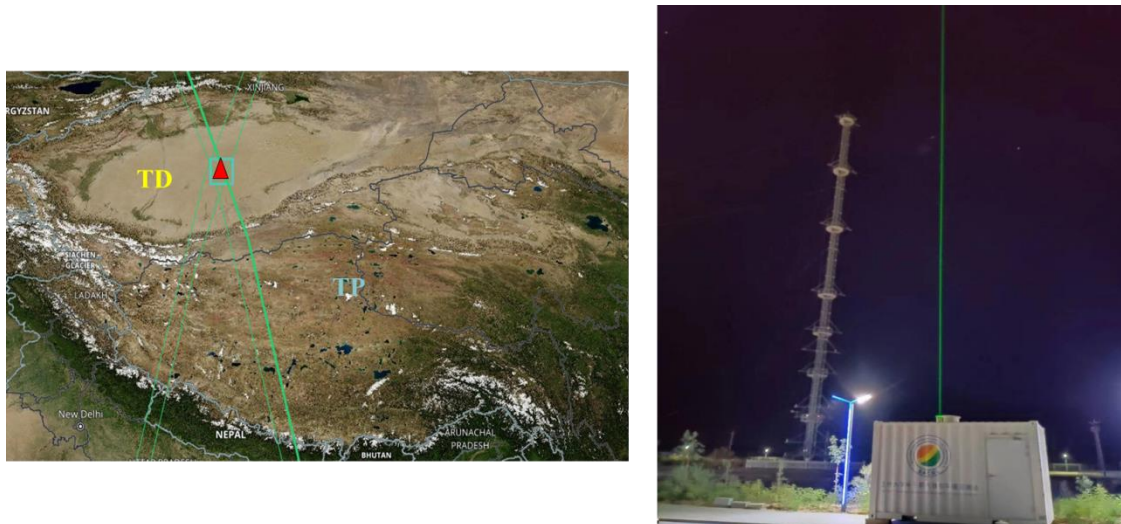
Figure 2. CALIPSO satellite orbit passes through the central area of the Taklimakan Desert hinterland-left (the red triangle represents the observation coordinates of the ground-based LIDAR - right (38.967 ° N, 83.65 ° E, 1099.3m), TD - Taklimakan Desert, TP - Qinghai Tibet Plateau) (pictures from NASA'S Earth data (left) and photography(right)).

Table 2. Basic technical specifications of LIDAR from the hinterland of the Taklimakan Desert (TD).

| Detection range | Spatial resolution | Laser wavelength | Laser energy | Pulse frequency |
|---|---|---|---|---|
| 0~20km | 7.5m | 532nm/1064nm | 100mJ | 20Hz |

In this study, based on the Level_2 aerosol profile data product (extinction coefficient, EC) for daytime and nighttime detected by CALIOP from 2007 to 2020, the low-reliability aerosol target (LRAT) is screened and eliminated. The aerosol characteristic data set with higher reliability over the TP is constructed, and the data set is verified and compared with MODIS and ground-based LIDAR to test its effectiveness and accuracy. Thus, the vertical structure of aerosol characteristics climatology with higher reliability over the TP can be obtained, providing adequate observation facts and a basis for the TP. All steps were implemented and was processed

341     as follows in figure 3.
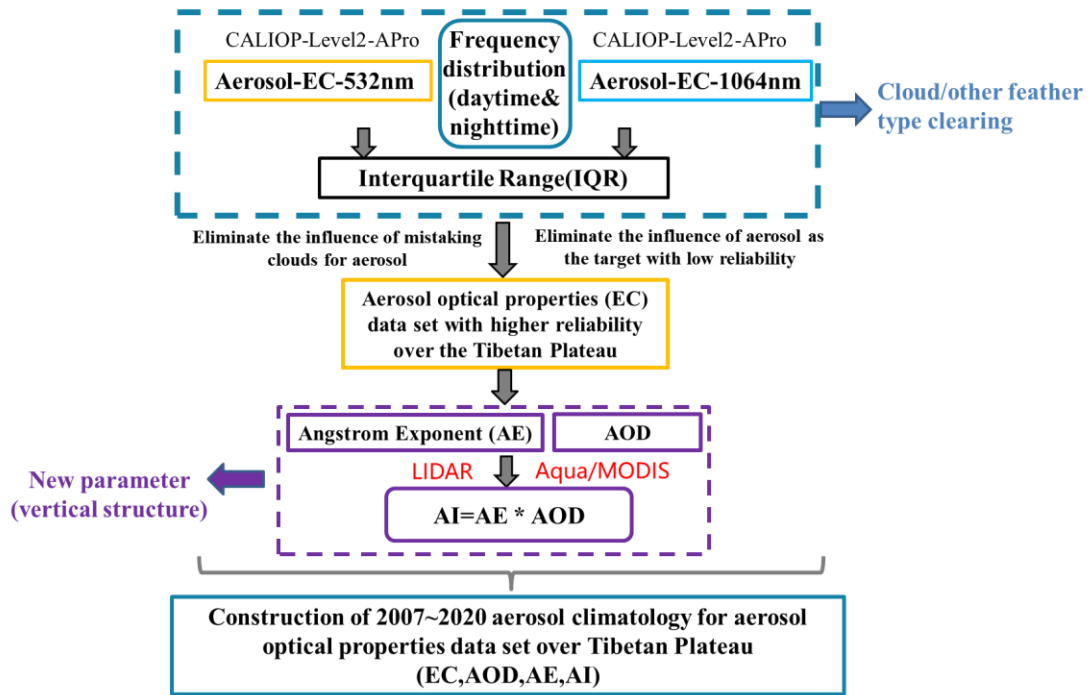
342

343 Figure 3. Flow chart of the aerosol characteristic data set construction and calculation process over

344 TP.

## 3 Results and analysis

### 3.1 Low-Reliability Aerosol Target (LRAT) screened and eliminate

347     In this section, we screened and eliminate LRAT for tropospheric aerosol

348 extinction coefficient (EC) from the available CALIOP profile products over the TP,

349 based on the statistical method (see Section 2.2). Figures 4 and 5 show the monthly

350 frequency distribution of EC at 532 nm and 1064 nm in the daytime during 2007-2020

351 from January to December was detected by the CALIPSO-CALIOP troposphere within

352 12 km. While figures 6 and 7 are for nighttime. Generally, figures 4-7 demonstrate the

353 non-normal distribution for EC. We found that the upper outlier appeared to remove

354 many enhanced aerosol measurements, when more sand and dust events occurred in the

355 surrounding areas and rose to the TP in spring and summer. In contrast, the extreme

356 outlier was effectively identified in the frequency distribution. Therefore, the extreme

357 outlier threshold used to clear LRAT observations from the CALIOP data set is

358 necessary.

After the LRAT of screened and eliminate, we can directly compare these measurements of the monthly climatology of data points and extreme outliers (2007－2020). We found that during the daytime for 532 nm and 1064 nm, the aerosol EC over the TP is mainly concentrated between 0 and 0.2. The extreme outliers in July and August are more significant than those in other months, which may be related to the rising motion of the TP as a heat source in summer to trigger convection, resulting in more ice clouds in the upper air, thus increasing the probability of misclassification the cirrus anvil as an aerosol (Carrió et al., 2007; Kojima et al., 2004; Seifert et al., 2007). Also, the aerosol data points (samples) is the largest in May and the smallest in November over TP; Obviously, spring and summer are more than autumn and winter; This is related to the frequent sand and dust activities in spring and summer around the TP (such as Taklimakan Desert) and anthropogenic pollution (as mentioned earlier).

Similarly, during the nighttime for 532nm and 1064nm, the aerosol EC over the TP is mainly concentrated between 0 and 0.1, and the extreme outliers in July and August are still greater and more significant than those in other months. Still, it is smaller than the daytime data set. The primary consideration is that the daytime solar noise is considerable and the signal-to-noise ratio of LIDAR observation is low, which further increases the probability that the aerosol EC presents skewed distribution; It can be seen that the removal of LRAT from daytime data is more conducive to improving the accuracy of data. Meanwhile, the aerosol data points are the largest in April and the smallest in December over the TP. It can be seen that in April (spring), more aerosol samples were lifted and transported to the TP. Numerous observations have shown elevated dust plumes lofted into the free troposphere during spring, and air parcels between 4 km and 7 km mainly originate from TD (Huang et al.,2008; Sasano,1996; Liu et al.,2008; Zhou et al.,2002; Matsuki et al., 2003). It is the same as the daytime with spring and summer being more than autumn and winter while there is one order of magnitude larger than the data point in the day. It is not difficult to see that the main reason is that the CALIOP is less sensitive during daytime than nighttime due to signal-noise-ratio reduction by solar background illumination, which leads to weakly scattering layers can be detected during nighttime while missed during daytime (Huang

389 et al., 2013; Liu et al.,2009).

390
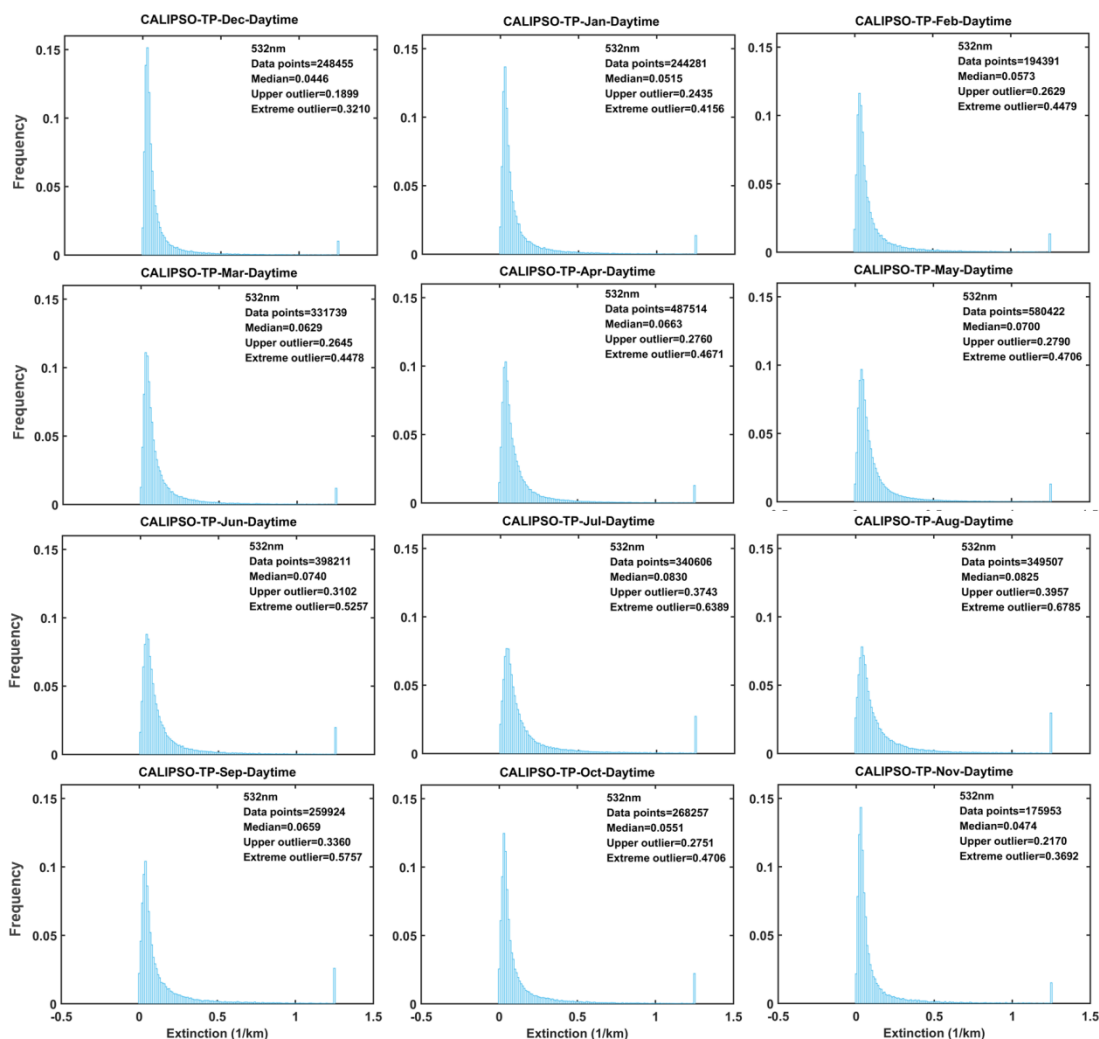
391

392 Figure 4. Monthly frequency distribution of aerosol extinction coefficient at 532nm over Tibet
393 Plateau (TP) daytime during 2007~2020 from January to December (Panels 1st stands for Winter for
394 Dec ~ Feb.; Panels 2nd stands for Spring for Mar ~ May; Panels 3rd stands for Summer for Jun ~
395 Aug; Panels 4th stands for Autumn for Sep ~ Nov). Frequency distribution is the number of events
396 normalized to the maximum value. Upper outlier and extreme outlier and median also have been
397 shown.

398

399

400

401

402

403
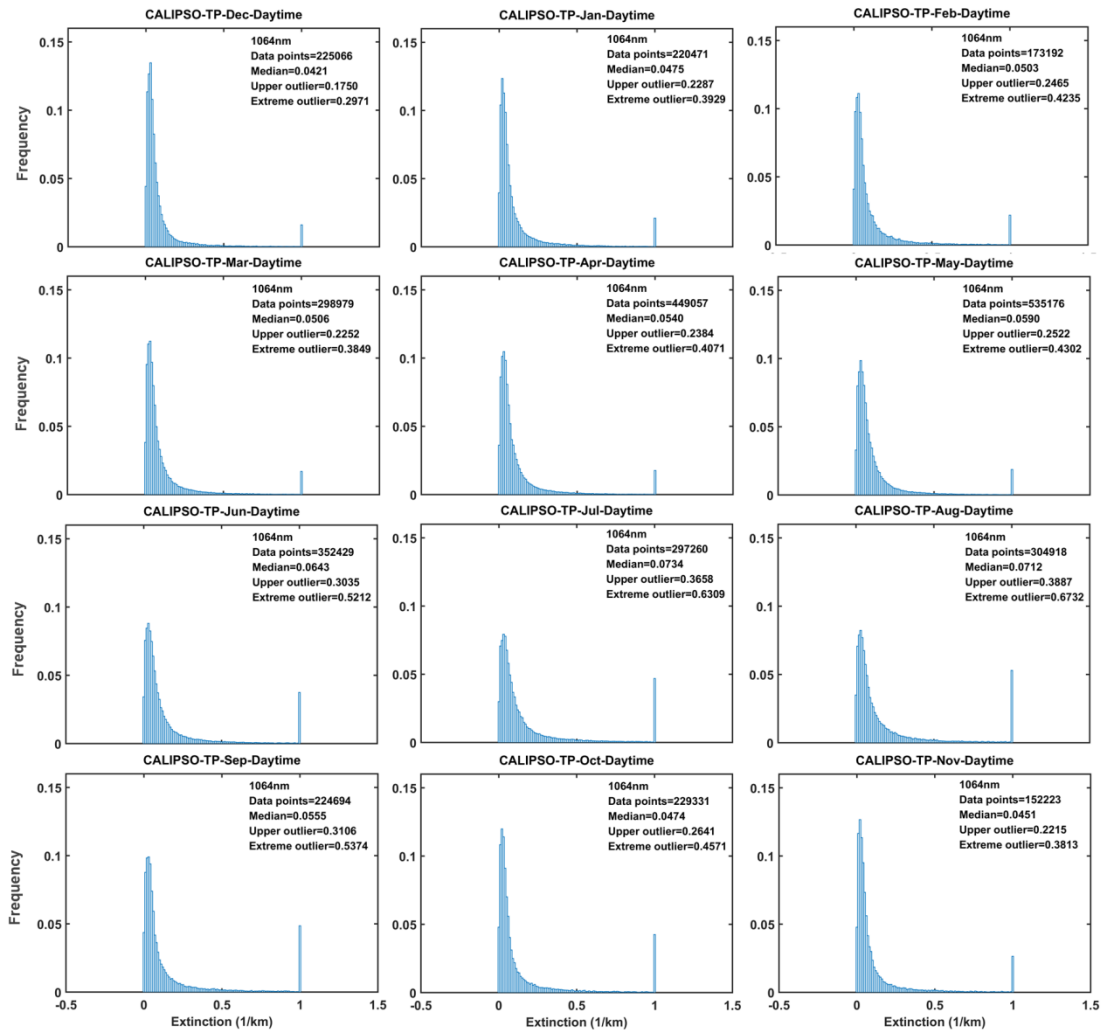
404
405 Figure 5. The same as in Figure 4 except for 1064nm.
406
407
408
409
410
411
412
413
414
415
416
417
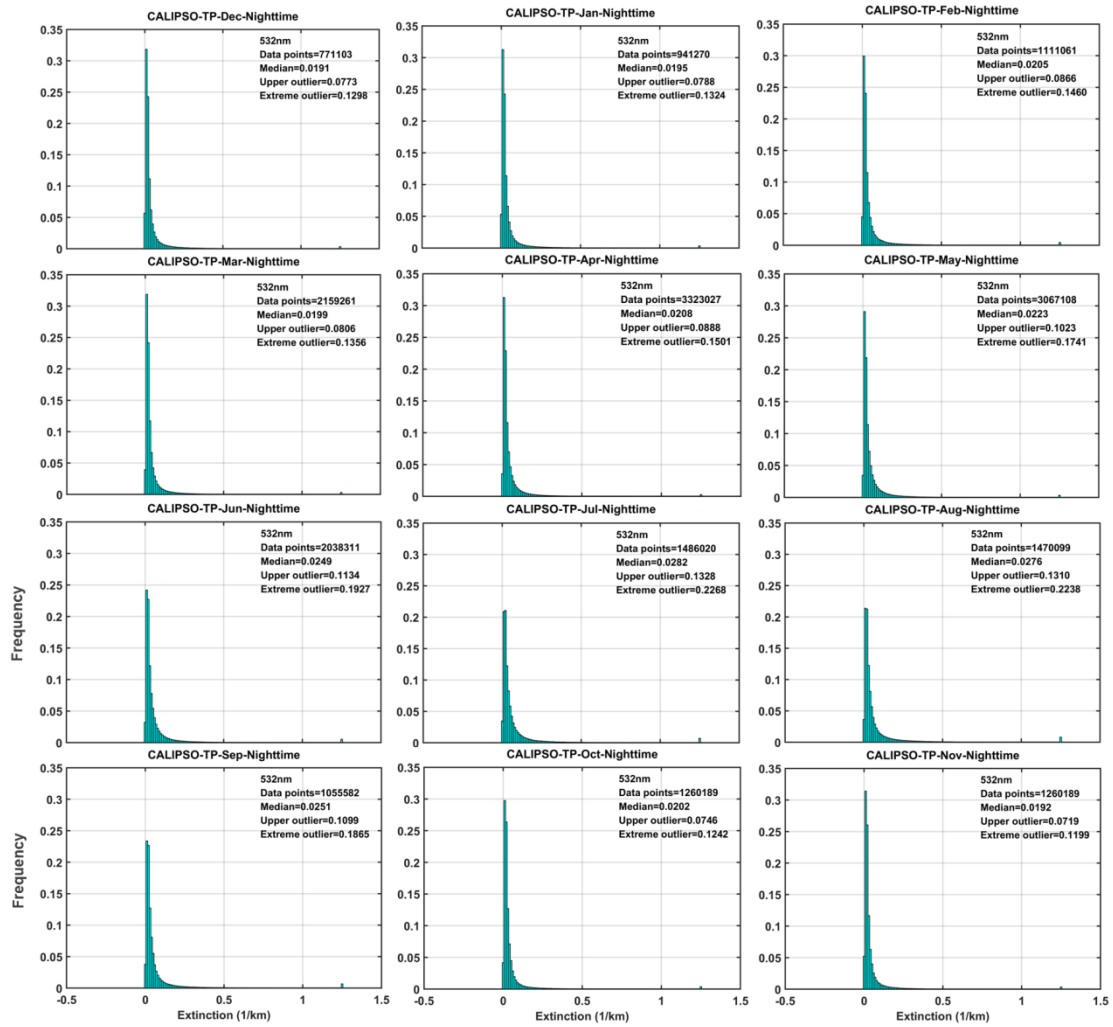
Figure 6. Frequency distribution of aerosol extinction coefficient at 532nm over Tibet Plateau (TP) nighttime during 2007-2020 from January to December (Panels 1st stands for Winter for December-February; Panels 2nd stands for Spring for March-May; Panels 3rd stands for Summer for June-August; Panels 4th stands for Autumn for September-November). Frequency distribution is shown as the number of events normalized to the maximum value. Upper outlier and extreme outlier, and median also have been shown.
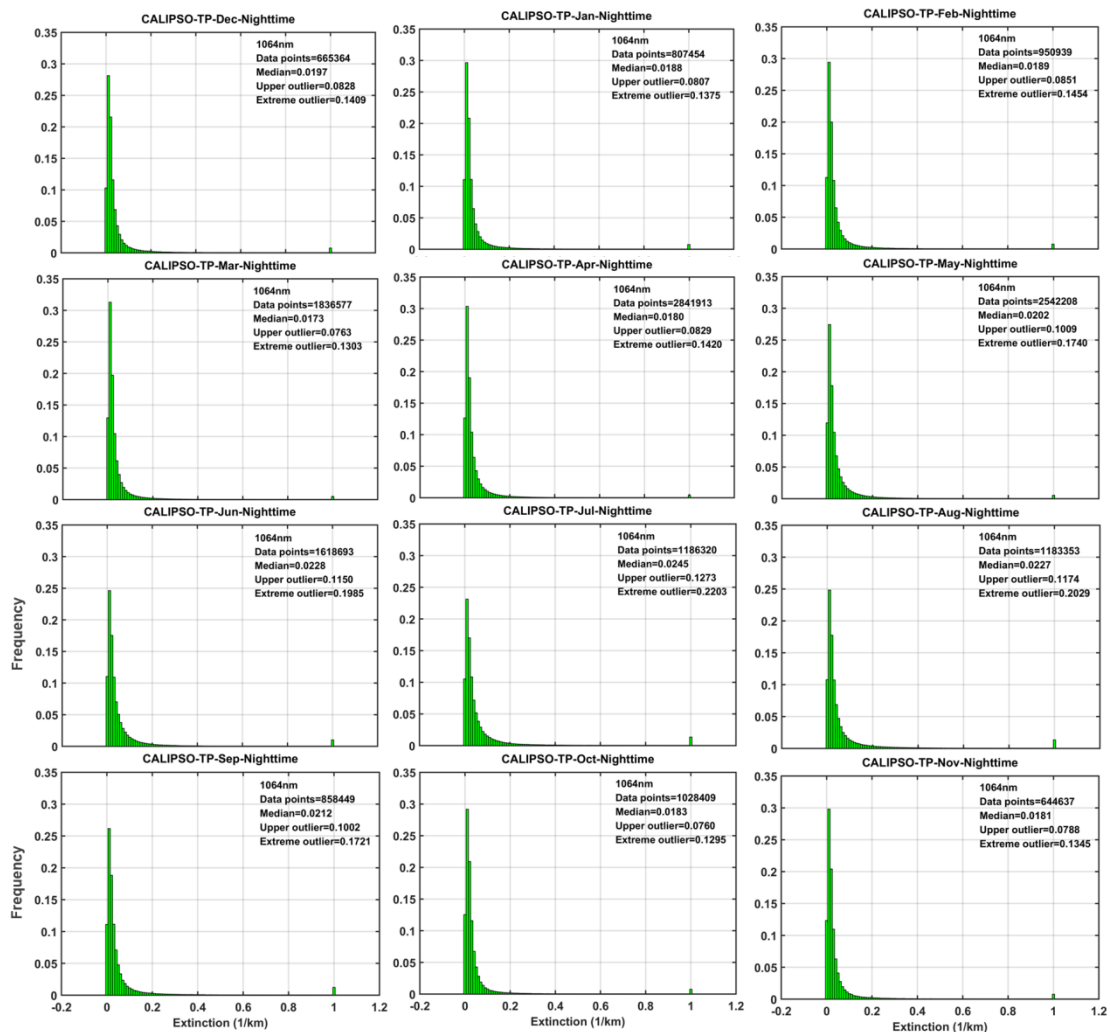
Figure 7. The same as in Figure 6 except for 1064nm.

### 3.2 Constructing vertical aerosol index (AI) for daytime and nighttime

Figures 8 and 9 show daytime altitude-latitude plots of the monthly climatology of the aerosol EC with 532 nm and 1064 nm before and after screen, respectively. The monthly mean climatology of the pseudo-Ångström exponent (AE) and Aerosol Index (AI) vertical structure is then computed (as shown in figure 10). We choose January, April, July and October to represent winter, spring, summer and autumn (same as below). Figures 8 and 9 show that extreme outliers in the troposphere over the TP have been eliminated, especially in the lower layer, where more obvious LRAT have been identified and eliminated. In the upper layer (more than 7 km), especially in April and July (i.e., spring and summer), weak cirrus signs may exist in the original aerosol signals and be eliminated. Compared with other seasons, the aerosol on the TP is widely and uniformly distributed in the troposphere in April, indicating that in general, more

445 aerosol loads are lifted over the TP in April. In figure 10, we compute values between

446 0 and -1 for much of the troposphere and occasionally are between 0 and 2 in the middle

447 troposphere (less than 8 km), which has similar results or pattern in Kovilakam's study

448 (Kovilakam et al., 2020). Note that the derived value for pseudo AE is without the

449 physical meaning, and it is simply a means to combine AOD to obtain AI of vertical

450 structure. Using this climatology of pseudo-AE values, we can effectively convert any

451 month of AI data to 532 nm and 1064 nm because the fixed AE is not necessarily

452 applicable to retrieving aerosol extinction in all months. Relevant research points out

453 that the accuracy has been improved, that is, using the corresponding AE index of each

454 month to correct the satellite data (Kovilakam et al., 2020).

455 Figure 10 also demonstrates the distribution characteristics of AI values at 532nm

456 and 1064nm in different seasons over the TP in the daytime. In all seasons, AI is mainly

457 distributed between -0.04 and 0.04. Still, the proportion between 0 and -0.02 is the

458 largest. Here, we have a broad understanding of traditional AI, the AI is a way to

459 measure how backscattered ultraviolet (UV) radiation from an atmosphere containing

460 aerosols differs from that of a pure molecular atmosphere (Guan et al., 2010). AI is

461 especially sensitive to the presence of UV absorbing aerosols such as smoke, mineral

462 dust, and volcanic ash. AI, positively suggests the existence of absorbent aerosols (dust,

463 black carbon, etc.); A small or negative AI suggests the presence of non-absorbable

464 aerosols or clouds) (Hu et al.,2020; Guan et al., 2010; Hammer et al., 2018). AI varies

465 with aerosol layer height, optical depth, and single scattering albedo (Torres et al.,

466 1998;2007; Hsu et al.,2004; Jeong and Hsu, 2008). However, the significance of

467 obtaining vertical structure AI in our research content is different from that of traditional

468 AI representation. The AI obtained from our research work cannot effectively

469 characterize the absorption and non-absorption of its aerosols, as the results we obtained

470 are in the non-ultraviolet band range, the aerosol concentration represented by the

471 vertical structure AI we obtained is not possessed by column AOD. Compared to the

472 aerosol column concentration AOD information, as AOD is an integral result of the

473 entire layer height, it will to some extent lose some of the true changes in the vertical

474 height of aerosols. The significance of our work is that the AI with higher reliability

475 obtained here can more effectively obtain aerosol concentration information at the

476 vertical height. In the four seasons, the distribution of aerosols in the north is broder

477 than that in the south; In spring, the rise height of aerosol is higher and the vertical

478 distribution range is more comprehensive; The elevation in summer is lower than that

479 in the other three seasons, but the aerosol species are more abundant, because there are

480 many ranges of AE values.

481
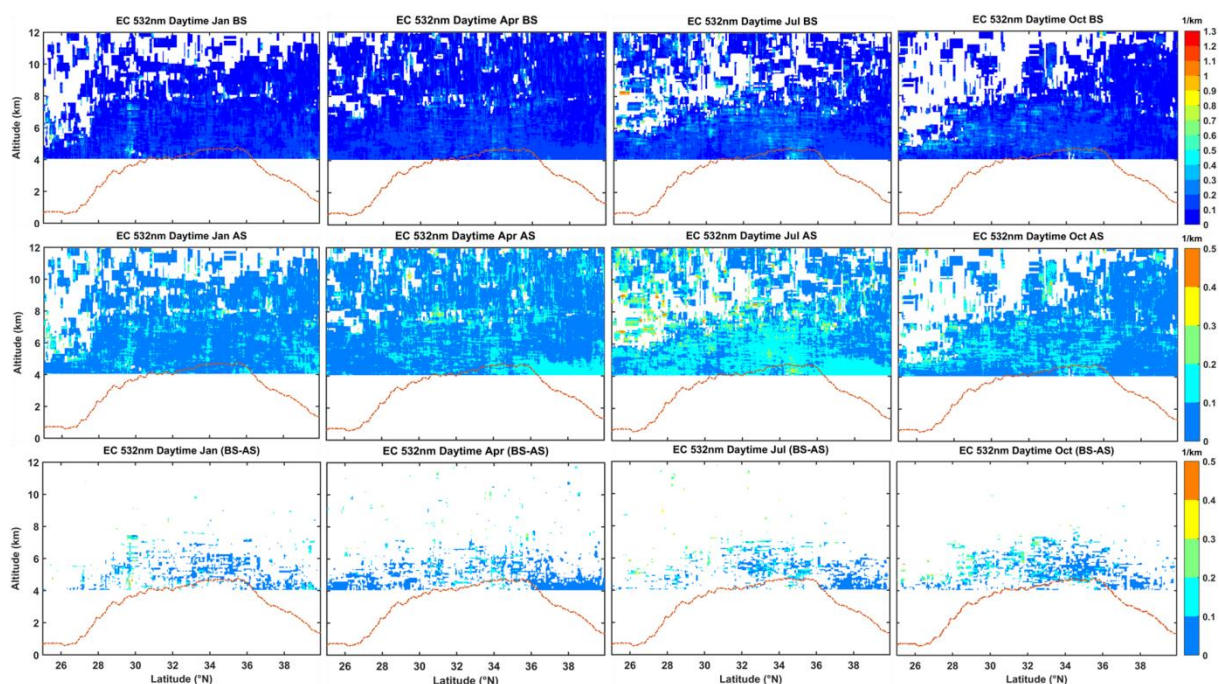
482

483 Figure 8. The monthly average comparison and difference of 532nm aerosol extinction coefficient
484 before and after low-reliability aerosol target (LRAT) removal over Tibet Plateau (TP) daytime
485 during 2007-2020. The reddish-brown dotted line denotes the surface. (BS: Before Screened, first
486 line; AS: After Screened, second line; (BS-AS) means Before Screened minus After Screened,
487 representing spatial lattice with screening and elimination, third line)

488
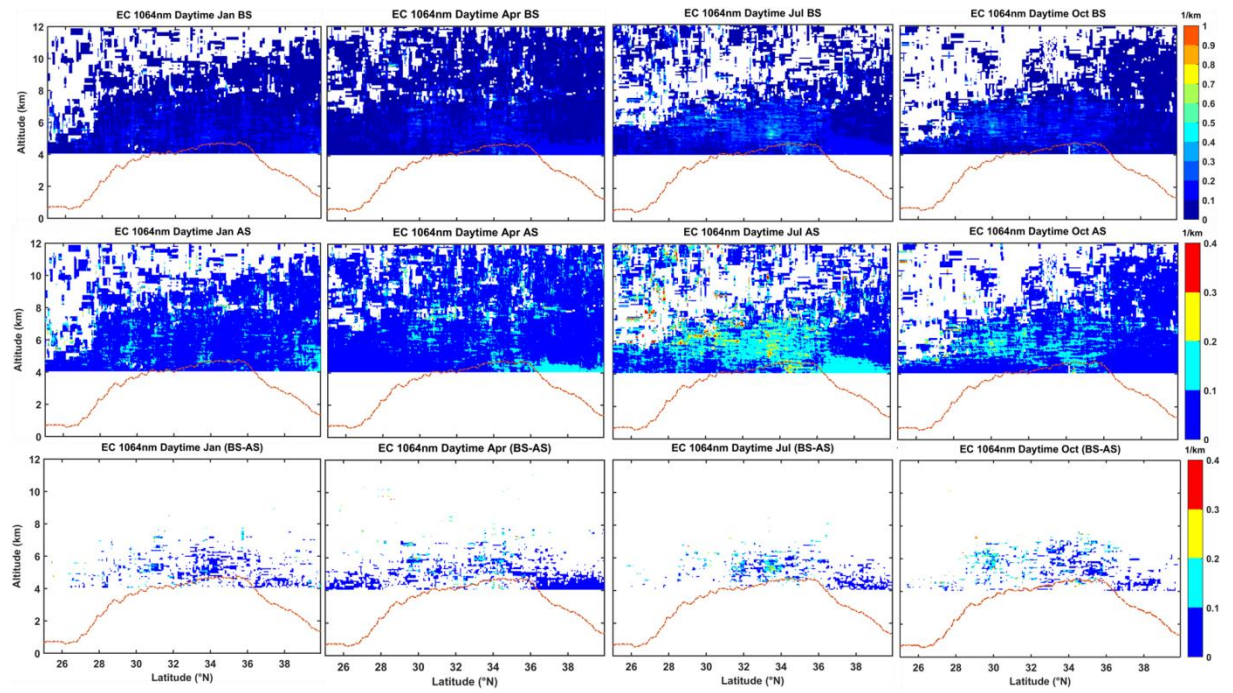
Figure 9. The same as in figure 8, but for 1064 nm.
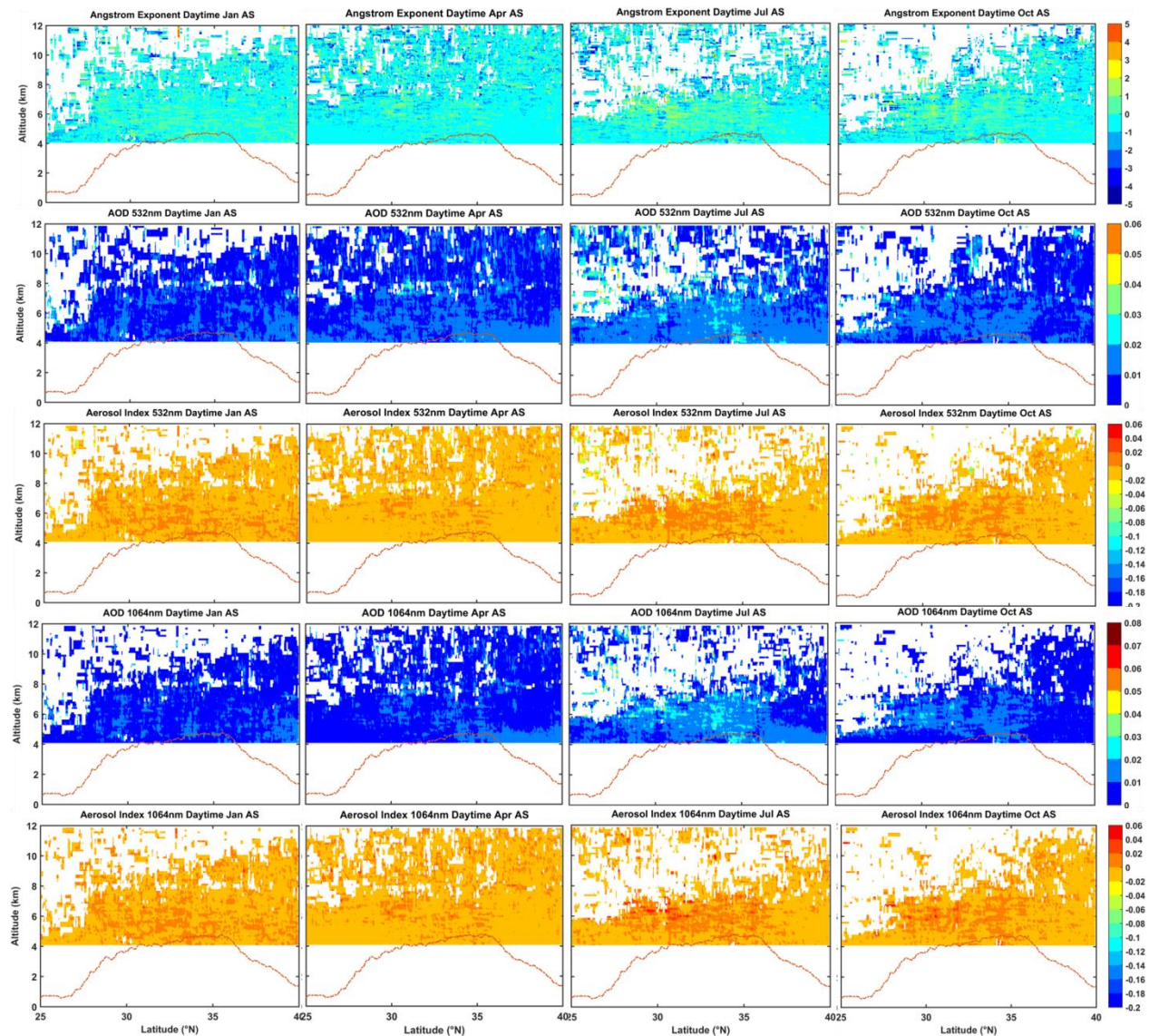
492

493 Figure 10. The monthly average construction of Angstrom Exponent (AE) and Aerosol Index (AI)

494 of vertical structure for 532nm & 1064nm over Tibet Plateau (TP) daytime during 2007-2020.

495

496    Similarly, figure 11 includes the nighttime difference plots between the before-

497 screened CALIOP 532nm EC and after-screened for different months during 2007-2020.

498 The difference before and after screening is immense, especially at the height of more

499 than 5 km in the southern region of the TP in July and October. We can see extreme

500 outliers in the troposphere over the TP that have been recognized and eliminated. The

501 EC detected at CALIOP 1064 nm shows a similar distribution characteristic as 532 nm,

502 and also includes the different attributes before and after the screened and removal of

503 LRAT (see as figure 12). In all seasons, AI is mainly distributed between -0.02 and 0.02.

504 Still, the proportion between 0 and -0.02 is the largest in April and July between 4 and

505 8km. Meanwhile, AI above 8 km is mainly concentrated at 0~0.02, indicating that

506 modal characteristics of vertical structure distribution of aerosol concentration and

507 diversity of aerosol types. It is worth noting that there is a large amount of aerosol over

508 the TP in January (winter), related to anthropogenic emissions of pollutants in winter

509 and fossil fuel combustion (such as black carbon and smoke). We note the pattern of AI

510 is more or less consistent with objective facts and phenomena.

511      Interestingly, compared with the daytime, the aerosol detected by CALIOP at night

512 can rise to a higher height and has a broader distribution range. It can be seen that

513 because the signal-to-noise ratio at night is higher than that in the daytime, CALIOP

514 can detect smaller particles, which is also why the quality and effectiveness of CALIOP

515 night detection data is better than that in the day. After a series of correction algorithms

516 and calculating relevant parameters, we have constructed the tropospheric AI

517 climatology dataset over the TP for 2007-2020.
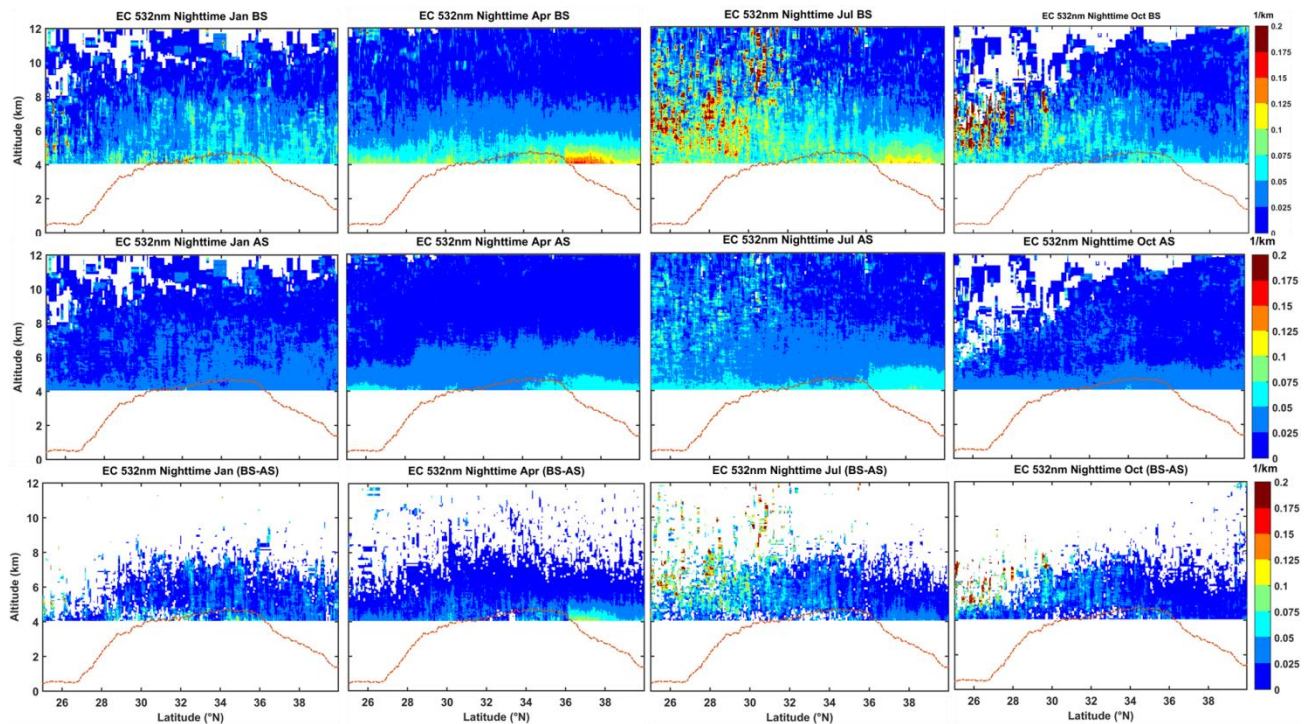
519 Figure 11. The same as in figure 8, but for nighttime.
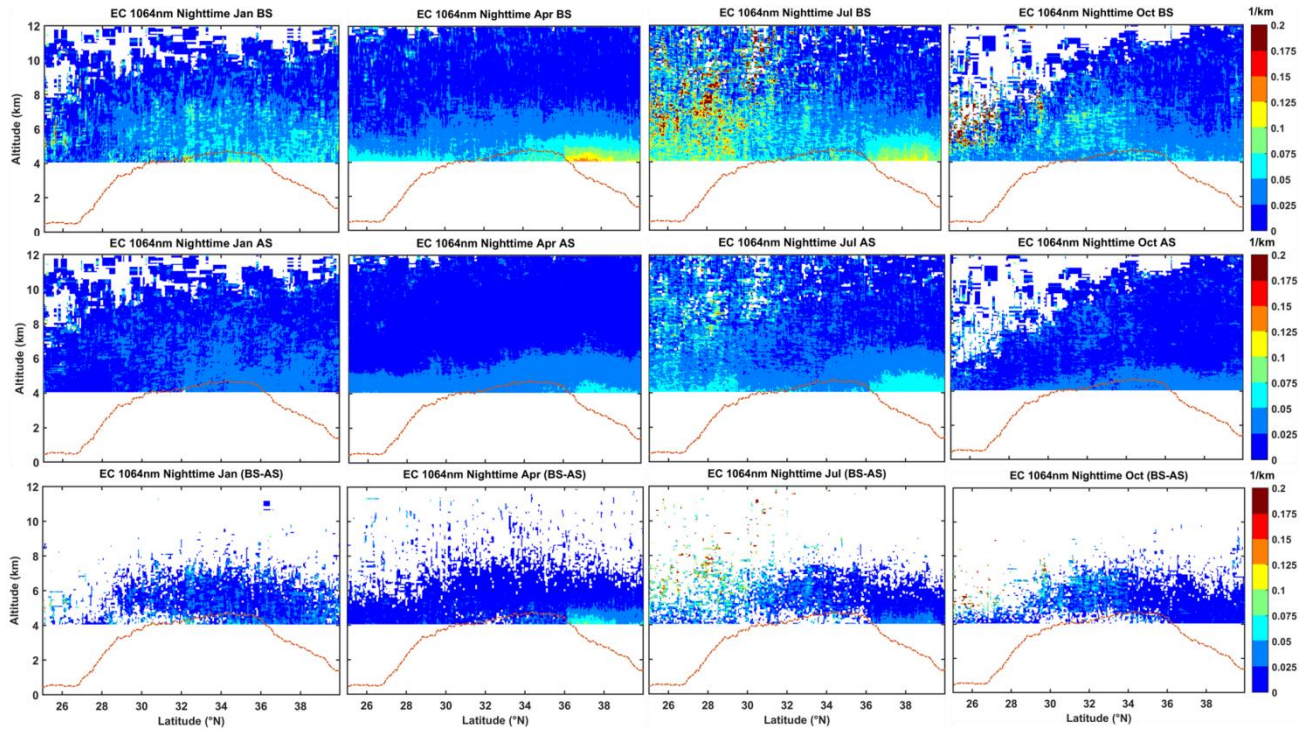
Figure 12. The same as in figure 11, but for 1064nm.
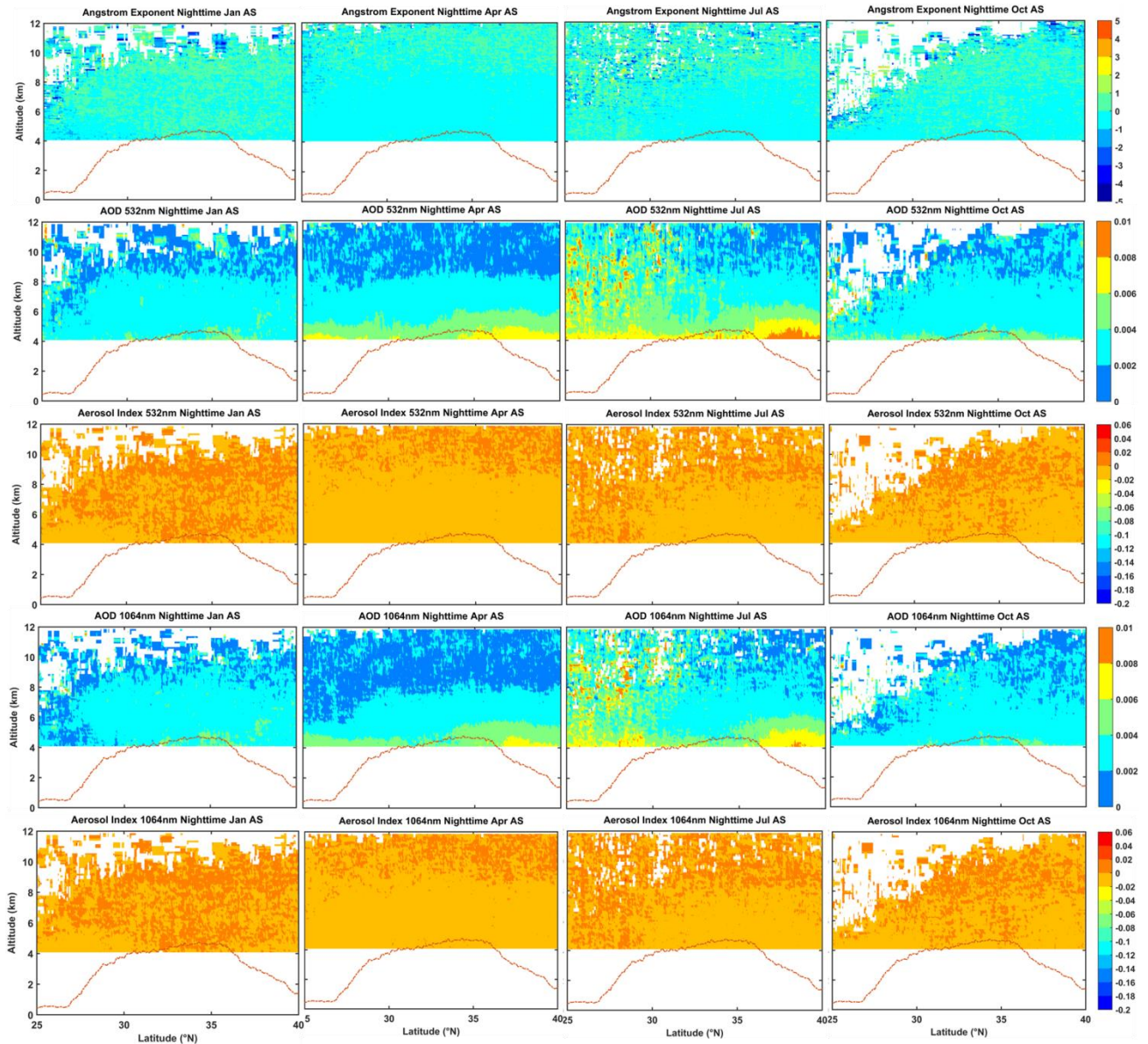
526

527 Figure 13. The same as in figure 10, but for nighttime.

### 3.3 Validation of the aerosol index (AI) dataset

#### 3.3.1 Comparisons with satellite Aqua-MODIS AI products

530      The multiyear monthly average spatial distributions of the AE and AOD from

531 MODIS have been shown in figure 14, and AI was also calculated (Figure 14). The

532 distribution of AE values over the TP in all seasons shows a decreasing trend from

533 southeast to northwest, indicating that the particles in the upper air of the southeast

534 region are dominated by small particles. In contrast, the particles in the upper air of the

535 northwest region are dominated by large particles, especially in April of spring, which

536 is related to the uplift and transmission of dust aerosol from the Taklimakan Desert to

the northern part the TP in spring. Additionally, we can see that the AE value of Taklimakan Desert in the north of the TP in April and July in spring and summer is smaller (as the source of the sand area, mainly dust aerosol), which is smaller than in January and October in autumn and winter; AOD and AE showed opposite seasonal variation distribution patterns. According to the spatial distribution pattern of AI calculated from MODIS detection results (AE and AOD), it can be seen that the AI value over the TP is mainly between 0 and 0.4.

Figure 14 also compares the normalized frequency distribution of AI over the TP exhibiting a significant difference in all seasons from MODIS and CALIOP between BS and AS. It is evident that, in general, compared with the actual data results without any processing, after removing the low-reliability aerosol target, the average AI value of CALIOP is closer to the result of MODIS, and the normalized frequency distribution pattern is closer to the same. Interestingly, the AI mean value and normalized frequency distribution pattern of CALIOP in April (spring) after removing the LRAT are more agreement and matched with the results of MODIS; In addition, the AI mean value and normalized frequency distribution pattern of CALIOP in July (summer), and October (autumn) is more consistent with the MODIS results, and both have apparent improvement; The difference between the AI average value of CALIOP in January (winter) and the result of MODIS is relatively more extensive, but the normalized frequency distribution pattern is more consistent. This may be related to the type and chemical composition of aerosol particles that rise over the TP in different seasons and the atmospheric climate conditions unique to the topography of the TP. In brief, the accuracy of aerosol parameters AI calculated after obtaining aerosol EC with higher reliability has been dramatically improved (more or less), so even though not completely accurate, this strategy is expected to reduce the inaccuracy of the computed AI at least.

Meanwhile, it is proved that using extreme outliers as a limit to get more reliable aerosol detection information is effective and reliable. It is important to note that the 550 nm wavelength range of MODIS belongs to the visible light range, and the data products provided at the satellite transit time are the daytime detection results.

567    Therefore, here we compare and verify the daytime detection results of CALIOP (532

568    nm) with MODIS results, which are consistent in time, close in detection wavelength,

569    comparable, and representative. In addition, the quality of CALIOP daytime detection

570    data is inferior to that at night, and the reliability and accuracy of the optimized data

571    are more effectively verified by comparison with the results of MODIS. Passive

572    techniques (i.e., MODIS) have the advantage of providing a 2-D distribution of AI over

573    a wide swath, during active strategies (i.e., CALIOP) with AI vertical structure. They

574    are complementary and have their advantages.

575

576

577

578

579

580

581

582

583

584

585

586

587

588

589

590

591

592

593
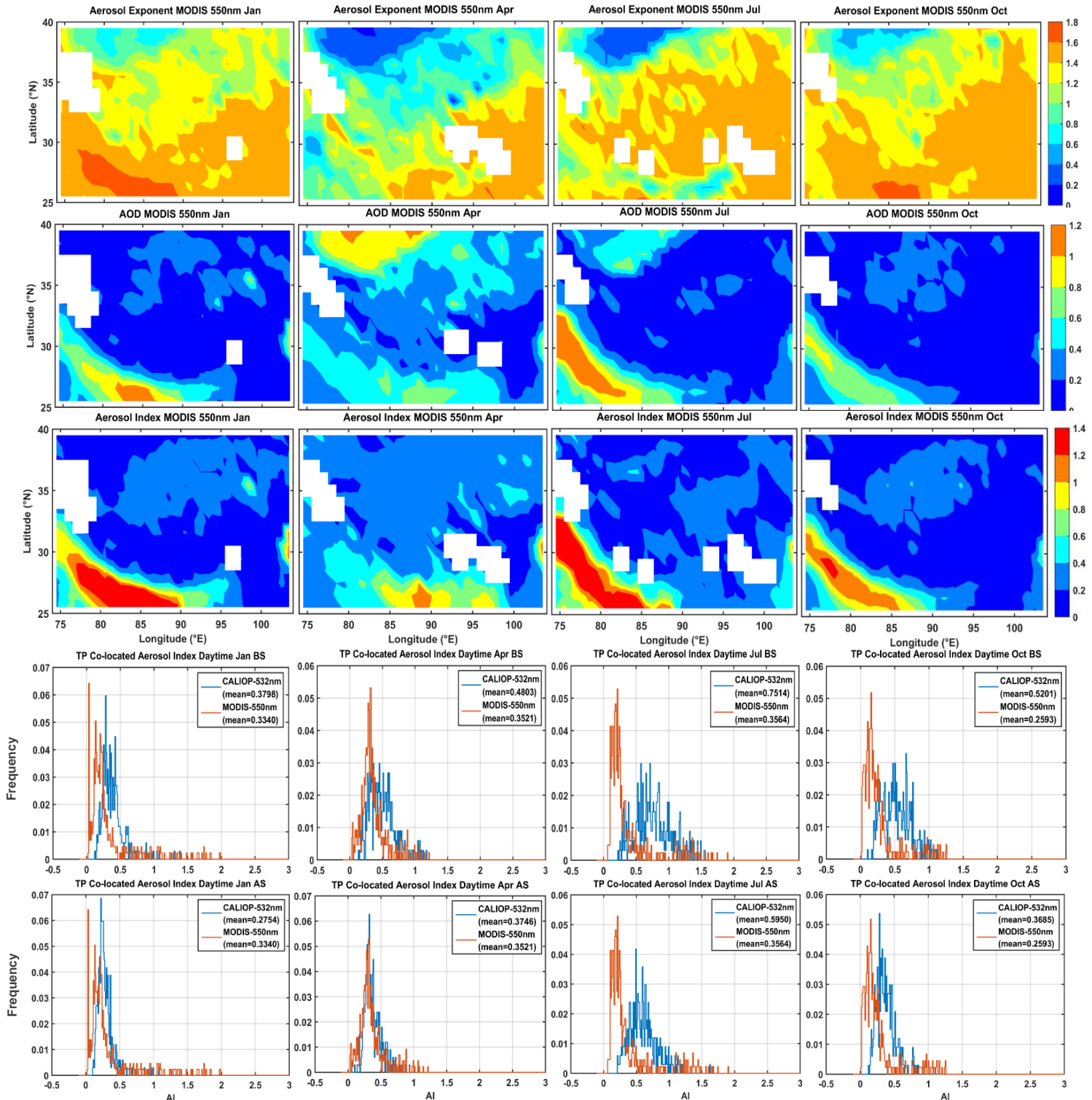
594    Figure 14. Frequency test of AI calculated by MODIS-based aerosol AE and AOD over the Qinghai

595    Tibet Plateau and AI calculated by CALIPSO-based aerosol AE and AOD with high reliability for

596    daytime (BS: Before Screened, the fourth line; AS: After Screened, the fifth line).

597    *3.3.2 Performance evaluation based on in-situ Lidar observations*

598        To further verify the performance of the AI product derived from CALIOP over

the TP, we chose to use the ground-based LIDAR observation results in the center of the Taklimakan Desert in the north of the TP to evaluate the effectiveness and accuracy of the AI vertical structure of CALIOP.

To match the transit time of ground-based LIDAR observation and satellite CALIOP observation, we extracted the EC (532 nm and 1064 nm) of ground-based LIDAR during the daytime and nighttime to match the CALIOP adjacent observation period, as shown in Figure 15 (observation case in TD on July 11, 2021, daytime: 03:00-05:00, night: 14:00-16:00, China Beijing time, UTC+8). Considering the daytime detection results of CALIOP for comparison and verification with MODIS in the above, to further strengthen the inspection of CALIOP optimization results, we still choose the daytime results of ground-based LIDAR detection for comparison and verification. From Figure 15, it can also be seen that there are clouds or other LRAT in the daytime high altitude in the ground-based LIDAR detection signal. This will be more beneficial for us to check the validity and reliability of the results of the elimination of LRAT and the calculated AI value.

Similarly, for ground-based LIDAR detection, we first reverse EC and use the IQR method (see sec.2.2) to obtain extreme outliers and identify and eliminate the LRAT (Figure 15). We can see that the LRAT (such as clouds and surface clutter etc.) are effectively eliminated after the data optimization of 532nm and 1064nm detection results EC. It is once again proved that it is effective and reliable to use extreme outliers as a limit to obtain more reliable aerosol detection information.
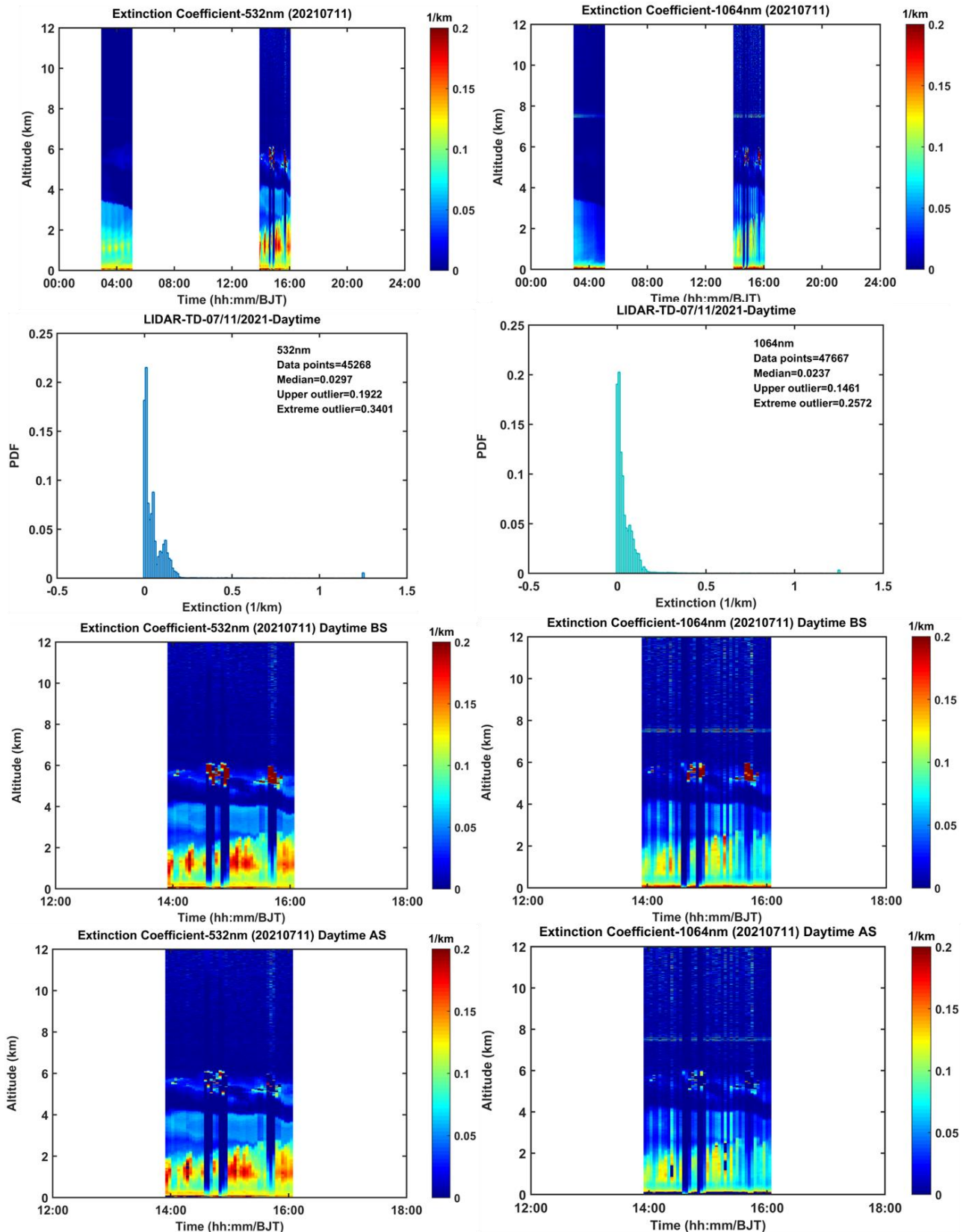
Figure 15. Removal of low-reliability aerosol target signals detected by ground-based LIDAR in the hinterland of Taklimakan Desert.

It is needed to be pointed out that the case of ground-based LIDAR detection on

628  July 11, 2021 is quite typical, but there is a significant deviation in satellite transit, and

629  this process cannot be well captured. To maximize and better match this process, we

630  take the ground-based LIDAR observation in the hinterland of the Taklimakan Desert

631  as the center (38.967 ° N, 83.65 ° E, 1099.3m), select 38.5~39.5 ° N and 83~84 ° E

632  range, extract the ECs observed by CALIOP transit in this range during the daytime

633  from 2007 to July 2020, and eliminate the LRAT. After averaging the optimized data,

634  further, calculate the AE value (as shown in Figure 16). Figure 16 depicts the detection

635  results of ground-based LIDAR and CALIOP optimal crossing point and the

636  comparison of calculated AI values. The AE values detected by ground-based LIDAR

637  and CALIOP are mainly distributed between - 1 and 1, and the proportion between - 1

638  and 0 is the largest. The aerosol can be raised to the height of 6 km, and the higher

639  concentration of aerosol is mainly concentrated below 2 km from the AOD vertical

640  layer, showing a decreasing trend with the increase of height; AI values are primarily

641  distributed between -0.02 and 0.02, and the average value and standard deviation trend

642  of AI change with height are also basically consistent. Generally, all those facts

643  demonstrate the agreement of the AI dataset with the CALIOP and ground-based

644  LIDAR. Besides, all the evidence shows that after removing the LRAT, the optimized

645  data can obtain aerosol characteristics with higher reliability.

646      Based on the monthly climatology AI product, we explored average vertical

647  structure change characteristics of AI over TP during 2007-2020 (as shown in figure

648  17). AI values in the daytime and at night over the TP mainly fluctuate around 0, and

649  the standard deviation increases with the increase of altitude. The trend of AI changes

650  with altitude is relatively consistent, and the standard deviation below 6 km is slight,

651  indicating that the dispersion of aerosol particles is small. However, the fluctuation in

652  the daytime is greater than that at night (the data quality at night is better than that in

653  the daytime). In general, the detection results of 532 nm and 1064 nm can achieve

654  complementary observation.

655      In general, the quality and robustness of the aerosol parameter product have

656  improved for EC and AI with some issues that still persist in the data set which we

657  mention below:

658    As we do not have ground-based LIDAR detection data on the TP, we have

659    selected grond-based LIDAR data from the center of the Taklamakan Desert for

660    verification and evaluation. The objectives of the verification and evaluation include

661    the removal of low reliability aerosol targets and the validation of the effectiveness and

662    rationality of the constructed aerosol AI parameter results. Due to the limited detection

663    data of ground-based LIDAR, we chose a typical aerosol process detected by ground-

664    based LIDAR (July 11, 2021), but it did not match well with the transit time and

665    scanning area of the CALIPSO satellite, resulting in significant errors. Therefore, we

666    choose to compare and verify the results of the average values of July in all years within

667    the central area of the transit Taklamakan Desert detected by CALIPSO (see the green

668    box on the left in Figure 2). Minimize spatial errors caused by significant differences

669    in spatial positions. This kind of error is inevitable in our data processing process and

670    will affect the consistency of detection results to some extent.

671    Besides, although the monthly based AI correction significantly improves the

672    comparison between CALIPSO and MODIS, we note somewhat a larger deviation

673    maybe occurs in winter, and the effect after correction in summer is the best and

674    significant, which may be related to the increased probability of mistaking clouds as

675    aerosol particles due to more convective activities in summer. This helps us to refine

676    our research on summer aerosols over the TP.

677

678

679

680

681

682

683

684

685

686
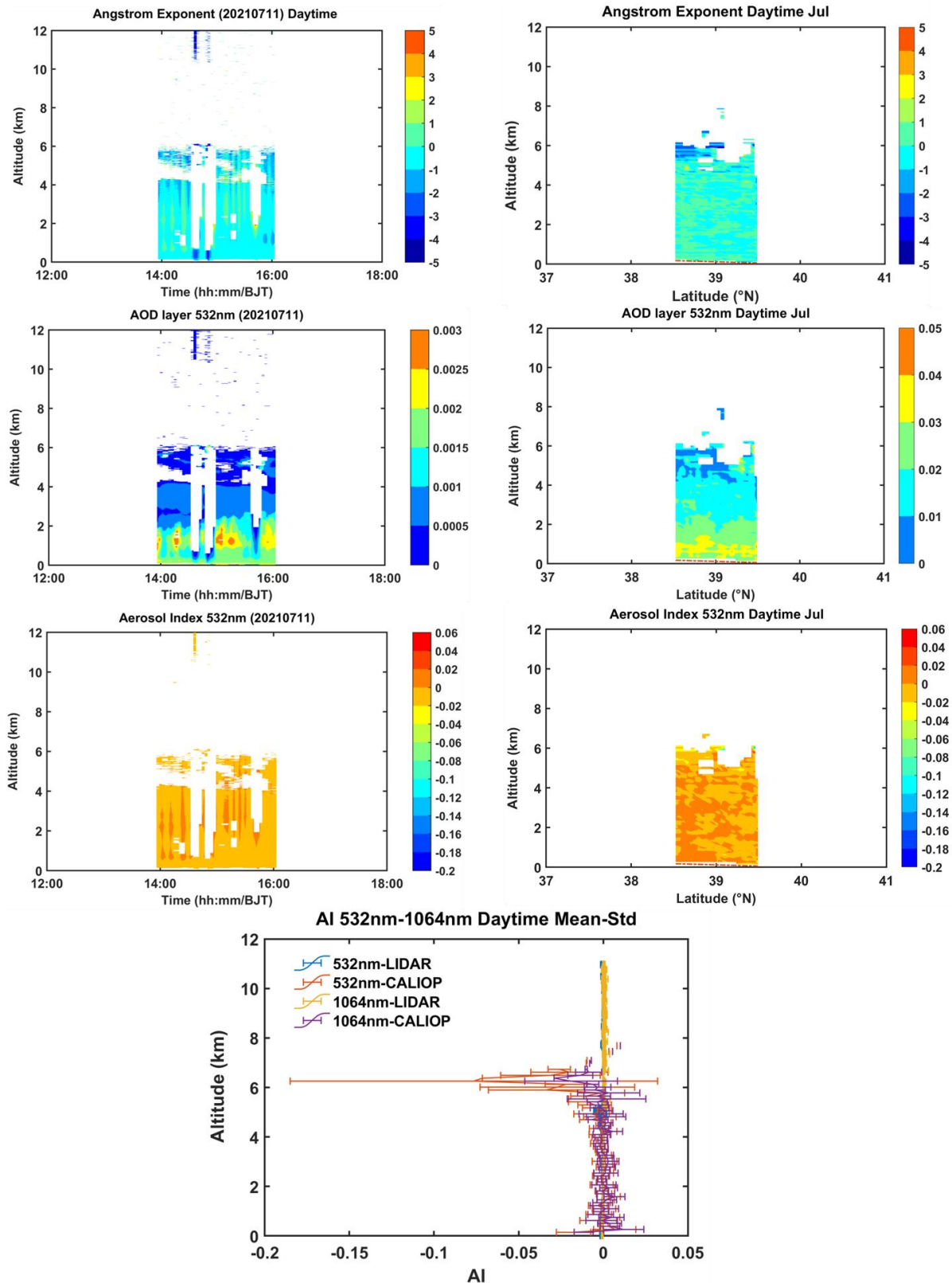
687    Figure 16. Comparative verification of AI of CALIPSO and ground-based LIDAR remote sensing

688    in Taklimakan Desert.

689
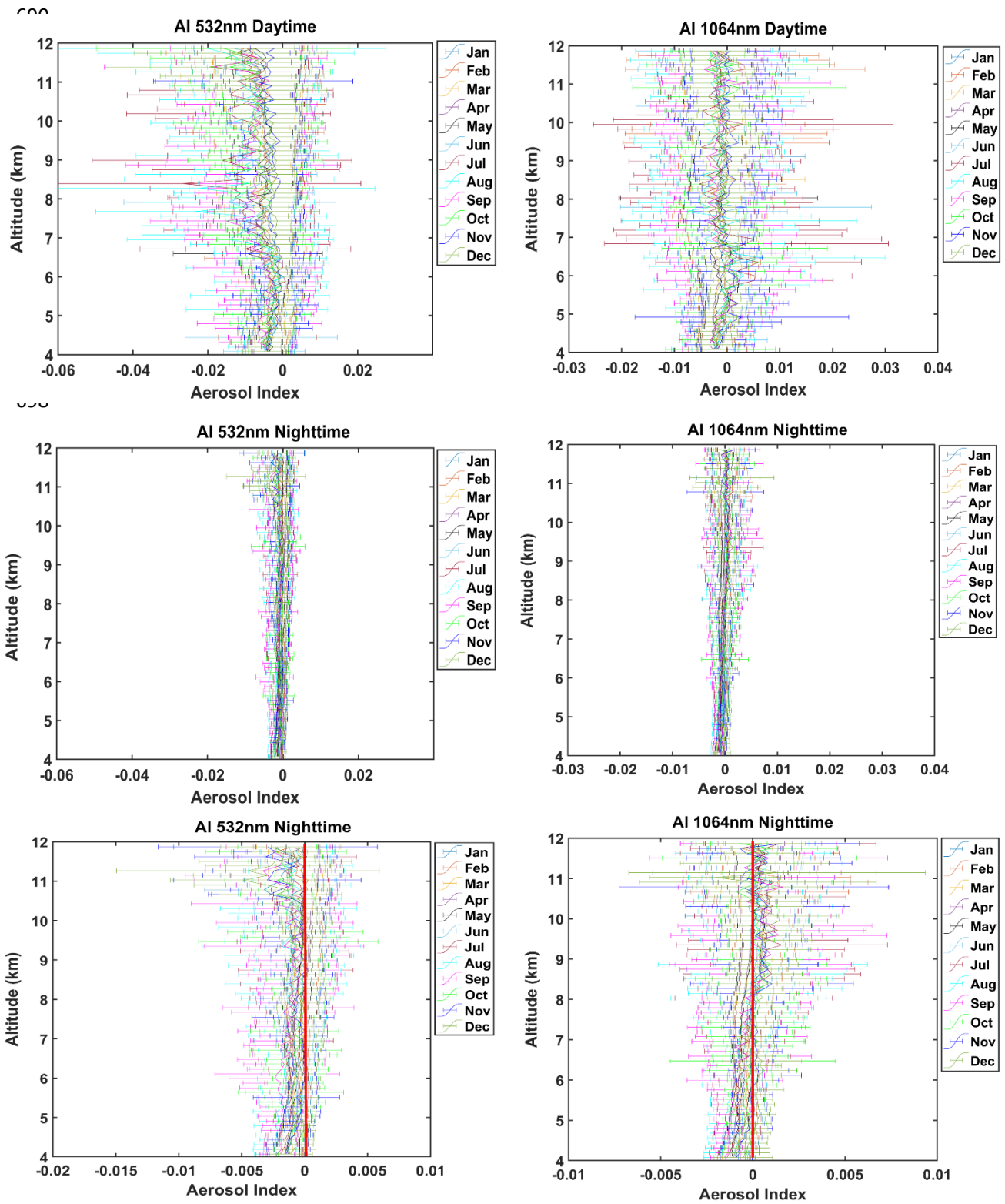
715     Figure 17. Monthly average vertical structure change characteristics of AI (mean & standard

716     deviation) over TP during 2007-2020.

717

718

719

**4 Data availability**

Data described in this work are available at https://data.tpdc.ac.cn/en/disallow/03fa38bc-25bd-46c5-b8ce-11b457f7d7fd

DOI:10.11888/Atmos.tpdc.300614. (Honglin Pan et al., 2023)

**5 Summary and outlook**

This present study is the first to report long-term, advanced-performance, high-resolution, continuous and high-quality, monthly climatology aerosol AI vertical structure from the CALIOP observation over TP which may be used to better understand aerosol radiation forcing under the background of accelerated climate change. Using the relationship developed when EC measurements are available, we screened the entire EC record. We assembled a climatology of high-altitude aerosol characteristics for daytime and nighttime from 2007 to 2020. In addition to providing a monthly climatology AI data set for MODIS and ground-based LIDAR validation, our data set also reveals the patterns and numbers of high-altitude vertical structure characteristics of the aerosol troposphere over the TP.

To produce an accurate and higher reliability of AI values, we applied several correction procedures and rigorously checked for data quality constraints during the long observation period spanning almost 14 years (2007-2020). Nevertheless, some uncertainties remain mainly due to technical constraints, as well as limited documentation of the measurements. Even though not completely accurate, this strategy is expected to at least reduce the inaccuracy of the computed characteristic value of aerosol optical parameters. Following this initial work, we obtained vertical AI value with higher reliability. This provides information about the vertical structures of aerosol that could be used in climate models. The collection of more reliable and robust research data sets of aerosol characteristics in these extreme environments is the key basis for promoting comprehensive research on the energy balance of ground-atmosphere radiation over the Tibetan Plateau and even the global region. We expect that this data set will help some current and future research to simulate the climate change of the monthly climatology. It will also help to update future data sets and study the interaction

of aerosol-cloud-precipitation, thus providing sufficient observation facts and basis.

Finally, it should be pointed out that the AI obtained in the ultraviolet channel can currently characterize both absorption and non-absorption aerosols. The AI obtained from our research work cannot effectively characterize the absorption and non-absorption of its aerosols, as the results we obtained are in the non-ultraviolet band range, which is also an area that we need to further explore in the future. However, the aerosol concentration represented by the vertical structure AI we obtained is not possessed by column AOD. The significance of our work is that the AI with higher reliability obtained here can more effectively obtain aerosol concentration information and also presents a diversity of aerosol types at the vertical height over TP. This is the main highlight of our research work. The reason why we use AI to test the results of MODIS and ground LIDAR is to verify the effectiveness and reliability of AI. Fortunately, the test results are very consistent and reasonable. Therefore, the AI of physical meaning here which can effectively characterize aerosol concentration information at vertical heights.

**Author contributions.** HP led the reprocessing of the CALIOP, LIDAR, MODIS measurements, data analysis and the preparation of the figures, with JH and JL both contributing to design of the paper and progression of figures and text of the article. ZH, MW and TZ made the original LIDAR measurements. ZH, AM and WH provided the dataset and advice on the re-processing of the LIDAR and CALIOP. KRK and FY contributed to either advising/co-ordinating the data recovery. All co-authors performed writing sections of the paper, and/or reviewing drafts of the paper.

**Competing interests.** The authors declare that they have no conflict of interest.

**Acknowledgements.**
We are grateful to the CALIPSO (https://eosweb.larc.nasa.gov/), MODIS (https://ladsweb.modaps.eosdis.nasa.gov/) instrument scientific teams at NASA for the provision of satellite data, and "Belt and Road" Lidar Network from Lanzhou University, China (http://ciwes.lzu.edu.cn/), which are available online and formed the central

780 database in the present work.

781

782 **Financial support.**

783 This work was financially Sponsored by Scientific and Technological Innovation Team

784 (Tianshan Innovation Team) Project of Xinjiang (Grant No. 2022TSYCTD0007), the

785 Second Tibetan Plateau Scientific Expedition and Research Program (STEP)(Grant No.

786 2019QZKK0602),the Natural Science Foundation of Xinjiang Uygur Autonomous

787 Region (Grant No. 2022D01B74), National Natural Science Foundation of China

788 (Grant No. 42005074), Scientific Research and Operation Cost Project of Urumqi

789 Institute of Desert Meteorological, China Meteorological Administration (Grant No.

790 IDM2020003).

791

792 **References**

793 Bucci, S., Cagnazzo, C., Cairo, F., Liberto, L.D., Fierli, F.: Aerosol variability and

794     atmospheric transport in the Himalayan region from CALIOP 2007–2010

795     observations, Atmospheric Chemistry and Physics, 14(9): 4369-4381, 2014.

796 Boos, W., Kuang, Z.: Dominant control of the South Asian monsoon by orographic

797     insulation versus plateau heating, Nature, 436, 218-222, 2010.

798 Buchard, V., Da Silva, A. M., Colarco, P. R., Darmenov, A., Randles, C. A., Govindaraju,

799     R., Torres, O., Campbell, J., Spurr, R.: Using the OMI aerosol index and absorption

800     aerosol optical depth to evaluate the NASA MERRA Aerosol Reanalysis,

801     Atmospheric Chemistry and Physics, 15(10), 5743-5760, 2015.

802 Chen, X., Zuo, H., Zhang, Z., Cao, X., Duan, J., Zhu, C., Zhang, Z., Wang, J.: Full-

803     coverage 250 m monthly aerosol optical depth dataset (2000–2019) amended with

804     environmental covariates by an ensemble machine learning model over arid and

805     semi-arid areas, NW China, Earth System Science Data, 14(12), 5233-5252, 2022.

806 Chen, S., Huang, J., Zhao, C., Qian, Y., Leung, L. R., Yang, B.: Modeling the transport

807     and radiative forcing of Taklimakan dust over the Tibetan Plateau: A case study in

808     the summer of 2006, Journal of Geophysical Research: Atmospheres, 118(2), 797-

809     812,2013.

Chen, S., Zhang, R., Mao, R., Zhang, Y., Chen, Y., Ji, Z., Gong, Y., Guan, Y.: Sources, characteristics and climate impact of light-absorbing aerosols over the Tibetan Plateau, Earth-Science Reviews, 232, 104111,2022.

Carrió, G. G., van Den Heever, S. C., Cotton, W. R.: Impacts of nucleating aerosol on anvil-cirrus clouds: A modeling study, Atmospheric research, 84(2), 111-131, 2007.

Guan, H., Esswein, R., Lopez, J., Bergstrom, R., Warnock, A., Follette-Cook, M., Iraci, L. T.: A multi-decadal history of biomass burning plume heights identified using aerosol index measurements, Atmospheric Chemistry and Physics, 10(14), 6461-6469, 2010.

Guan, H., Chatfield, R. B., Freitas, S. R., Bergstrom, R. W., Longo, K. M.: Modeling the effect of plume-rise on the transport of carbon monoxide over Africa with NCAR CAM, Atmos. Chem. Phys., 8, 6801–6812, doi:10.5194/acp-8-6801-2008, 2008.

Goldberg, D. L., Gupta, P., Wang, K., Jena, C., Zhang, Y., Lu, Z., Streets, D. G.: Using gap-filled MAIAC AOD and WRF-Chem to estimate daily PM2:5 concentrations at 1 km resolution in the Eastern United States, Atmos. Environ., 199, 443–452, https://doi.org/10.1016/j.atmosenv.2018.11.049, 2019.

Giles, D. M., Sinyuk, A., Sorokin, M. G., Schafer, J. S., Smirnov, A., Slutsker, I., Eck, T. F., Holben, B. N., Lewis, J. R., Campbell, J. R., Welton, E. J., Korkin, S. V., and Lyapustin, A. I.: Advancements in the Aerosol Robotic Network (AERONET) Version 3 database – automated near-real-time quality control algorithm with improved cloud screening for Sun photometer aerosol optical depth (AOD) measurements, Atmos. Meas. Tech., 12, 169–209, https://doi.org/10.5194/amt-12-169-2019, 2019.

Guan, H., Esswein, R., Lopez, J., Bergstrom, R., Warnock, A., Follette-Cook, M., Fromm, M., Iraci, L. T.: A multi-decadal history of biomass burning plume heights identified using aerosol index measurements, Atmospheric Chemistry and Physics, 10(14), 6461-6469, 2010.

Hsu, N. C., Si-Chee, T., King, M. D., Herman, J. R.: Aerosol properties over bright-reflecting source regions, IEEE Trans. Geosci. Rem. Sens., 42, 557–569, 2004.

840      Hammer, M. S., Martin, R. V., Li, C., Torres, O., Manning, M., Boys, B. L.: Insight into
841          global trends in aerosol composition from 2005 to 2015 inferred from the OMI
842          Ultraviolet Aerosol Index, Atmospheric Chemistry and Physics, 18(11), 8097-
843          8112, 2018.

844      Hu, Q., Wang, H., Goloub, P., Li, Z., Veselovskii, I., Podvin, T.,Li, K., Korenskiy, M.:
845          The characterization of Taklamakan dust properties using a multiwavelength
846          Raman polarization lidar in Kashi, China, Atmospheric Chemistry and Physics,
847          20(22), 13817-13834, 2020.

848      Hu, Y.,S.Rodier,K.Xu,W.Sun,J.Huang,B.Lin,P.Zhai,and D.Josset.: Occurrence,liquid
849          water content, and fraction of supercooled water clouds from combined
850          CALIOP/IIR/MODIS measurements, J.Geophys.Res., 115, D00H34,
851          doi:10.1029/2009JD012384, 2010.

852      Huang, L., Jiang, J. H., Tackett, J. L., Su, H., Fu, R.: Seasonal and diurnal variations of
853          aerosol extinction profile and type distribution from CALIPSO 5-year
854          observations, Journal of Geophysical Research: Atmospheres, 118(10), 4572-4596,
855          2013.

856      Huang, J., Minnis, P., Chen, B., Huang, Z., Liu, Z., Zhao, Q., Yi, Y., Ayers, J. K.: Long-
857          range transport and vertical structure of Asian dust from CALIPSO and surface
858          measurements during PACDEX, Journal of Geophysical Research: Atmospheres,
859          113(D23), 2008.

860      Immerzeel, W., Van Beek, L., Bierkens, M.: Climate change will affect the Asian water
861          towers, Science, 328 (5984), 1382-1385, 2010.

862      IPCC: Climate Change 2013: The Physical Science Basis. Contribution of Working
863          Group I to the Fifth Assessment Report of the Intergovernmental Panel on Climate
864          Change, edited by: Stocker, T. F., Qin, D., Plattner, G.-K., Tignor, M., Allen, S. K.,
865          Boschung, J., Nauels, A., Xia, Y., Bex, V., and Midgley, P. M., Cambridge
866          University Press, Cambridge, United Kingdom and New York, NY, USA, 1535 pp.,
867          2013.

868      IPCC, 2021: Climate Change 2021: The Physical Science Basis. Contribution of
869          Working Group I to the Sixth Assessment Report of the Intergovernmental Panel

on Climate Change, edited by: Masson-Delmotte, V., P. Zhai, A. Pirani, S.L. Connors, C. Péan, S. Berger, N. Caud, Y. Chen, L. Goldfarb, M.I. Gomis, M. Huang, K. Leitzell, E. Lonnoy, J.B.R. Matthews, T.K. Maycock, T. Waterfield, O. Yelekçi, R. Yu, and B. Zhou (eds.)]. Cambridge University Press, Cambridge, United Kingdom and New York, NY, USA, In press, doi:10.1017/9781009157896.

Iglewicz, B. and Hoaglin, D.: How to Detect and Handle Outliers, ASQC basic references in quality control, ASQC Quality Press, Milwaukee, 1993.

Kovilakam, M., Thomason, L. W., Ernest, N., Rieger, L., Bourassa, A., Millán, L.: The global space-based stratospheric aerosol climatology (version 2.0): 1979–2018, Earth System Science Data, 12(4), 2607-2634, 2020.

Kahn, R. A., Gaitley, B. J., Garay, M. J., Diner, D. J., Eck, T. F., Smirnov, A., Holben, B. N.: Multiangle Imaging SpectroRadiometer global aerosol product assessment by comparison with the Aerosol Robotic Network, J. Geophys. Res.-Atmos., 115, D23209, doi:10.1029/2010jd014601, 2010.

Kojima, T., Buseck, P. R., Wilson, J. C., Reeves, J. M., Mahoney, M. J.: Aerosol particles from tropical convective systems: Cloud tops and cirrus anvils, Journal of Geophysical Research: Atmospheres, 109(D12), 2004.

Kim, M.H., Omar, A.H., Tackett, J.L., Vaughan, M.A., Winker, D.M., Trepte, C.R., Hu, Y.,Liu, Z., Poole, L.R., Pitts, M.C., Kar, J., Magill, B.E.: The CALIPSO Version 4 Automated Aerosol Classification and Lidar Ratio Selection Algorithm, Atmospheric Measurement Techniques, 11(11):6107-6135,2018.

Liu, Y., Huang, J., Wang, T., Li, J., Yan, H., He, Y.: Aerosol-cloud interactions over the Tibetan Plateau: An overview, Earth-Science Reviews, 104216, 2022.

Liu, Y., Li, Y., Huang, J., Zhu, Q., Wang, S.: Attribution of the Tibetan Plateau to northern drought, National Science Review, 7(3), 489-492, 2020.

Liu, Y., Hua, S., Jia, R., Huang, J.: Effect of aerosols on the ice cloud properties over the Tibetan Plateau, Journal of Geophysical Research: Atmospheres, 124(16), 9594-9608, 2019.

Luo, H., Yanai, M.: The large-scale circulation and heat sources over the Tibetan Plateau and surrounding areas during the early summer of 1979, Part II: Heat and

moisture budgets, Mon. Wea. Rev., 112, 966–989, 1984.

Liou, K.: Influence of cirrus clouds on weather and climate processes: a global perspective, Mon. Weather Rev., 114, 1167–1199,1986.

Liu, Z., Kar, J., Zeng, S., Tackett, J., Vaughan, M., Avery, M., Pelon, J., Getzewich, B., Lee, K.P., Magill, B., Omar, A., Lucker, P., Trepte,C., Winker, D.: Discriminating between clouds and aerosols in the caliop version 4.1 data products, Atmos. Meas. Tech., 12, 703–734, 2019.

Liu, D., Z. Wang, Z. Liu, D. Winker, C. Trepte.: A height resolved global view of dust aerosols from the first year CALIPSO lidar measurements, J. Geophys. Res., 113, D16214, doi:10.1029/2007JD009776, 2008.

Liu, Z., Liu, D., Huang, J., Vaughan, M., Uno, I., Sugimoto, N., Kittaka, C., Trepte, C., Wang, Z., Hostetler, C., Winker, D.: Airborne dust distributions over the Tibetan Plateau and surrounding areas derived from the first year of CALIPSO lidar observations, Atmospheric Chemistry and Physics, 8(16), 5045-5060, 2008.

Liu, P. F., C. S. Zhao, Q. Zhang, Z. Z. Deng, M. Y. Huang, X. C. Ma, X. X. Tie.: Aircraft study of aerosol vertical distributions over Beijing and their optical properties, Tellus, Ser. B, 61(5), 756–767, doi:10.1111/j.1600-0889.2009.00440.x, 2009.

Molnar,P., Boos,W., Battisti, D.: Orographic controls on climate and paleoclimate of Asia: thermal and mechanical roles for the Tibetan Plateau, Annu. Rev. Earth Pl.Sc., 38 (1), 77-102, 2010.

Matsuki, A., Iwasaka, Y., Osada, K., Matsunaga, K., Kido, M., Inomata, Y., Trochkine, D., Nishita, C., Nezuka, T., Sakai,T., Zhang,D., Kwon, S. A.: Seasonal dependence of the long‐range transport and vertical distribution of free tropospheric aerosols over east Asia: On the basis of aircraft and lidar measurements and isentropic trajectory analysis, Journal of Geophysical Research: Atmospheres, 108(D23), 2003.

Nieberding, F., Wille, C., Fratini, G., Asmussen, M. O., Wang, Y., Ma, Y., Sachs, T.: A long-term (2005–2019) eddy covariance data set of $CO_2$ and $H_2O$ fluxes from the Tibetan alpine steppe, Earth System Science Data, 12(4), 2705-2724, 2020.

Nakajima, T., Higurashi, A., Kawamoto, K., Penner, J. E.: A possible correlation

between satellite‐derived cloud and aerosol microphysical parameters, Geophysical Research Letters, 28 (7), 1171-1174, https://doi.org/10.1029/2000GL012186, 2001.

Pan, H., Huo, W., Wang, M., Zhang, J., Meng, L., Kumar, K. R., Devi, N. L.: Insight into the climatology of different sand-dust aerosol types over the Taklimakan Desert based on the observations from radiosonde and A-train satellites, Atmospheric Environment, 238, 117705, 2020.

Qiu, J.: China: The third pole, Nature, 454, 393-396, https://doi.org/10.1038/454393a, 2008.

Rossow, W., Schiffer, R.: Advances in understanding clouds from ISCCP, Bull. Am. Meteorol. Soc., 80, 2261–2287, 1999.

Rieger, L. A., Bourassa, A. E., Degenstein, D. A.: Merging the OSIRIS and SAGE II stratospheric aerosol records, J. Geophys. Res. Atmos., 120, 8890–8904, https://doi.org/10.1002/2015JD023133, 2015.

Rieger, L. A., Zawada, D. J., Bourassa, A. E., Degenstein, D. A.: A Multiwavelength Retrieval Approach for Improved OSIRIS Aerosol Extinction Retrievals, J. Geophys. Res.-Atmos., 124, 7286–7307, https://doi.org/10.1029/2018JD029897, 2019.

Seifert, P., Ansmann, A., Müller, D., Wandinger, U., Althausen, D., Heymsfield, A. J., Massie, S.T., Schmitt, C.: Cirrus optical properties observed with lidar, radiosonde, and satellite over the tropical Indian Ocean during the aerosol-polluted northeast and clean maritime southwest monsoon, Journal of Geophysical Research: Atmospheres, 112(D17), 2007.

Sasano, Y.: Tropospheric aerosol extinction coefficient profiles derived from scanning lidar measurements over Tsukuba, Japan from 1990 to 1993, Appl. Opt., 35(24), 4941–4952, 1996.

Thomason, L. W. and Vernier, J.-P.: Improved SAGE II cloud/aerosol categorization and observations of the Asian tropopause aerosol layer: 1989–2005, Atmos. Chem. Phys., 13, 4605–4616, https://doi.org/10.5194/acp-13-4605-2013, 2013.

Twomey, S.A.: The influence of pollution on the shortwave albedo of clouds, J. Atmos.

Sci., 34 (7), 1149－1154,1977.

Torres, O., Bhartia, P. K., Herman, J. R., Ahmad, Z., and Gleason, J.: Derivation of aerosol properties from satellite measurements of backscattered ultraviolet radiation: Theoretical basis, J. Geophys. Res., 103, 17099–17110, doi:10.1029/98JD00900, 1998.

Torres, O., Tanskanen, A., Veihelmann, B., Ahn, C., Braak, R., Bhartia, P. K., Veefkind, P., Levelt, P.: Aerosols and surface UV products from Ozone Monitoring Instrument observations: An overview, J. Geophys. Res., 112, D24S47, doi:10.1029/2007JD008809, 2007.

Vernier, J. P., Fairlie, T. D., Natarajan, M., Wienhold, F. G., Bian, J., Martinsson, B. G., Crumeyrolle, S., Thomason, L.W., Bedka, K. M.: Increase in upper tropospheric and lower stratospheric aerosol levels and its potential connection with Asian pollution, Journal of Geophysical Research: Atmospheres, 120(4), 1608-1619, 2015.

Wan, B., Gao, Z., Chen, F., Lu, C.: Impact of Tibetan Plateau surface heating on persistent extreme precipitation events in Southeastern China, Mon. Weather Rev., 145 (9), 3485–3505, 2017.

Winker, D. M., Vaughan, M. A., Omar, A., Hu, Y., Powell, K. A., Liu, Z., Hunt, W. H., and Young, S. A.: Overview of the CALIPSO mission and CALIOP data processing algorithms, J. Atm. Ocean. Techn., 26, 2310–2323, 2009.

Winker, D.M., Hunt, W.H., McGill, M.J.: Initial performance assessment of CALIOP, Geophys. Res. Lett., 34, L19803, https://doi.org/10.1029/2007GL030135, 2007.

Wu, G., Zhang, Y.: Tibetan Plateau forcing and the timing of the monsoon onset over South Asia and the South China Sea, Mon. Wea. Rev., 126, 913-927,1998.

Wu, G., Liu, Y., Zhang, Q., Duan, A., Wang, T., Wan, R., Liu, X., Li, W., Wang, Z., Liang, X.: The influence of mechanical and thermal forcing by the Tibetan Plateau on Asian climate, J. Hydro. Meteor. Spec. Sect., 8 (4), 770-789, 2007.

Wu, G., Liu, Y., Dong, B., Liang, X., Duan, A., Bao, Q., Yu, J.: Revisiting Asian monsoon formation and change associated with Tibetan Plateau forcing: I. Formation, Climate dynamics, 39, 1169-1181, 2012.

Wu, G., Duan, A., Liu, Y., Mao, J., Ren, R., Bao, Q., He, B., Liu, B., Hu, W.: Tibetan Plateau climate dynamics: recent research progress and outlook, Natl. Sci. Rev., 2 (1), 100-116, 2015.

Wei, X., Bai, K., Chang, N.-B., Gao, W.: Multi-source hierarchical data fusion for high-resolution AOD mapping in a forest fire event, International Journal of Applied Earth Observation and Geoinformation, 102, 102366, https://doi.org/10.1016/j.jag.2021.102366, 2021.

Xu, X., Lu, C., Shi, X., Gao, S.: World water tower: an atmospheric perspective, Geophys. Res. Lett., 35 (20), 2008.

Xu, C., Ma, Y. M., You, C., Zhu, Z. K.: The regional distribution characteristics of aerosol optical depth over the Tibetan Plateau, Atmospheric Chemistry and Physics, 15(20), 12065-12078, 2015.

Yanai, M., Li, C., Song, Z.: Seasonal heating of the Tibetan Plateau and its effects on the evolution of the Asian summer monsoon, J. Meteor. Soc. Japan 70, 319-351,1992.

Zhang, S., Huang, Z., Li, M., Shen, X., Wang, Y., Dong, Q., Bi J., Zhang J., Li W., Li Z., Song, X.: Vertical structure of dust aerosols observed by a ground-based raman lidar with polarization capabilities in the center of the Taklimakan desert, Remote Sensing, 14(10), 2461, 2022.

Zhang, S., Huang, Z., Alam, K., Li, M., Dong, Q., Wang, Y., Shen, X., Bi, J., Zhang, J., Li, W., Li, Z., Wang, W., Cui, Z., Song, X.: Derived Profiles of CCN and INP Number Concentrations in the Taklimakan Desert via Combined Polarization Lidar, Sun-Photometer, and Radiosonde Observations, Remote Sensing, 1–20. https://doi.org/10.3390/rs15051216, 2023.

Zhou, J., G. Yu, C. Jin, F. Qi, D. Liu, H. Hu, Z. Gong, G. Shi, T. Nakajima, T. Takamura.: Lidar observations of Asian dust over Hefei, China in Spring 2000, J. Geophys. Res., 107(D15), 4252, doi:10.1029/,2002.2001JD000802, 2002.